

# Spatially Distinct Pools of TORC1 Balance Protein Homeostasis

Riko Hatakeyama,<sup>1</sup> Marie-Pierre Péli-Gulli,<sup>1</sup> Zehan Hu,<sup>1</sup> Malika Jaquenoud,<sup>1</sup> Guillermo Miguel Garcia Osuna,<sup>1</sup> Alessandro Sardu,<sup>1</sup> Jörn Dengjel,<sup>1,2</sup> and Claudio De Virgilio<sup>1,3,\*</sup>

<sup>1</sup>Department of Biology, University of Fribourg, 1700 Fribourg, Switzerland

<sup>2</sup>Department of Dermatology, Medical Center, University of Freiburg, 79104 Freiburg, Germany

<sup>3</sup>Lead Contact

\*Correspondence: [claudio.devirgilio@unifr.ch](mailto:claudio.devirgilio@unifr.ch)

## SUMMARY

The eukaryotic TORC1 kinase is a homeostatic controller of growth that integrates nutritional cues and mediates signals primarily from the surface of lysosomes or vacuoles. Amino acids activate TORC1 via the Rag GTPases that combine into structurally conserved multi-protein complexes such as the EGO complex (EGOC) in yeast. Here we show that Ego1, which mediates membrane-anchoring of EGOC via lipid modifications that it acquires while traveling through the trans-Golgi network, is separately sorted to vacuoles and perivacuolar endosomes. At both surfaces, it assembles EGOCs, which regulate spatially distinct pools of TORC1 that impinge on functionally divergent effectors: vacuolar TORC1 predominantly targets Sch9 to promote protein synthesis, whereas endosomal TORC1 phosphorylates Atg13 and Vps27 to inhibit macroautophagy and ESCRT-driven microautophagy, respectively. Thus, the coordination of three key regulatory nodes in protein synthesis and degradation critically relies on a division of labor between spatially sequestered populations of TORC1.

## INTRODUCTION

The eukaryotic target of rapamycin complex 1 (TORC1) is a central, homeostatic controller of growth that is often dysregulated in human diseases, including cancer, type 2 diabetes, and neurodegeneration (Albert and Hall, 2015; Eltschinger and Loewith, 2016; Saxton and Sabatini, 2017). TORC1 senses amino acids via the conserved Rag guanosine triphosphatases (GTPases) that form heterodimers of Gtr1 and Gtr2 in yeast or RAGA (or RAGB) and RAGC (or RAGD) in higher eukaryotes (Binda et al., 2009; Kim et al., 2008; Sancak et al., 2008). When abundant, amino acids favor the TORC1-activating state of these heterodimers that consists of guanosine triphosphate (GTP)-bound Gtr1/RAGA/B and guanosine diphosphate (GDP)-bound Gtr2/RAGC/D, while amino acid limitation inverts the GTP and GDP-loading status within these heterodimers and causes

TORC1 inactivation (Binda et al., 2009; Demetriades et al., 2014; Gao and Kaiser, 2006; Kim et al., 2008; Sancak et al., 2008). Rag GTPases function within larger protein assemblies, which are called the EGO complex (EGOC) in yeast or Regulator-Rag GTPase complex in mammals and are predominantly anchored to vacuolar and lysosomal membranes through their N-terminally lipidated Ego1 and p18/LAMTOR1 subunits, respectively (Binda et al., 2009; Powis et al., 2015; Sancak et al., 2010). In amino acid-fed mammalian cells, Rag GTPases recruit TORC1 to lysosomes, where the RHEB GTPase can allosterically activate the kinase activity of TORC1 (Yang et al., 2017; for a review, see Jewell and Guan, 2013), whereas yeast Rag GTPases regulate the constitutively vacuolar membrane-associated fraction of TORC1 independently of the RHEB-ortholog Rhb1 (Powis and De Virgilio, 2016). Yeast EGOC and TORC1 also colocalize to perivacuolar foci, which so far have not been assigned to any known subcellular structure or physiological function (Binda et al., 2009; Kira et al., 2016; Sturgill et al., 2008).

TORC1 adjusts growth to amino acid availability by balancing the equilibrium between protein synthesis and degradation. In yeast, TORC1 stimulates protein expression globally by activating ribosome biogenesis and protein translation through the AGC-family kinase Sch9, which, analogous to S6 kinases (S6K1/2) in mammals, is directly phosphorylated by TORC1 at the vacuolar membrane (Jin et al., 2014; Urban et al., 2007). Conversely, TORC1 inhibits bulk protein degradation through phosphorylation of Atg13 (at an elusive location) to prevent its association with Atg1 and consequently inhibit the induction of macroautophagy (Kamada et al., 2010). TORC1 further controls, through mechanisms that remain incompletely understood, the half-life of specific plasma membrane proteins by regulating their ubiquitin-mediated endocytosis and subsequent passage through the ESCRT (endosomal sorting complex required for transport)-dependent multivesicular body (MVB) pathway that destines them for lysosomal proteolysis (Boeckstaens et al., 2014; Jones et al., 2012; MacGurn et al., 2011). The ESCRT machinery is also required for the microautophagic degradation of vacuolar membrane-resident proteins (e.g., the lysine permease Ypq1, the V-ATPase subunit Vph1, and the alkaline phosphatase Pho8) when cells are starved for nutrients (Oku et al., 2017; Zhu et al., 2017). Both processes, namely, the channeling of membrane proteins through the endosomal MVB pathway and the degradation of vacuolar membrane proteins through microautophagy, require the initial clustering of ubiquitinated cargo

**Table 1. Mutant Alleles that Suppress the Gtr1<sup>S20L</sup>-Mediated Growth Defect**

Protein/Protein Complex	Mutant Allele <sup>a</sup>
EGOC	Ego1 <sup>N175fs</sup> , Ego1 <sup>R9*</sup> Ego3 <sup>A49P</sup> Gtr2 <sup>E42*</sup> , Gtr2 <sup>E185*</sup> , Gtr2 <sup>C231W</sup> , Gtr2 <sup>L283fs</sup>
TORC1	Tor1 <sup>A1928D</sup> Tco89 <sup>Q140fs</sup>
HOPS	Vam6 <sup>Q391*</sup> Vps41 <sup>N465fs</sup> Vps33 <sup>L18P</sup> Vps11 <sup>Q76*</sup>
AP-3	Apl6 <sup>M1V</sup> , Apl6 <sup>M613R</sup> Apm3 <sup>W31*</sup>
Palmitoyl-transferase	Akr1 <sup>W725*</sup>

<sup>a</sup>Stop codons are marked with an asterisk, and frameshift mutations are denoted with fs. See also Figure S1.

proteins by the heterodimeric Vps27-Hse1 ESCRT-0 complex. When cells grow in nutrient-rich medium, this complex is predominantly tethered to endosomes through the phosphatidylinositol 3-phosphate (PI3P)-binding Fab1, YOTB, Vac1, and EEA1 (FYVE) domain in Vps27 (Henne et al., 2011), but it may transit to the vacuolar rim when cells are starved for nutrients. Because Vps27 is unstable in starved cells (Dauner et al., 2017; Dobzinski et al., 2015), an open question in the field is whether TORC1 may control the localization and/or the stability of ESCRT-0.

Here, we show that Ego1 is delivered from the trans-Golgi network (TGN) to the vacuole mainly through the alkaline phosphatase (ALP) trafficking pathway that requires the AP-3 adaptor complex. In parallel, Ego1 is also routed via the monomeric clathrin adaptor proteins Gga1/2 to perivacuolar foci that we identify as perivacuolar endosomes harboring TORC1. Ego1 assembles EGOCs both at the vacuole and on endosomes to regulate two functionally distinct pools of TORC1 that target distinct effector proteins locally. Accordingly, vacuolar TORC1 preferentially phosphorylates Sch9, which associates with the vacuolar membrane through its affinity for phosphatidylinositol 3,5-bisphosphate (PI[3,5]P<sub>2</sub>) (Jin et al., 2014; Takeda et al., 2018). Endosomal TORC1, in contrast, predominantly phosphorylates its known substrate Atg13 to inhibit macroautophagy, as well as Vps27, which we pinpoint as a hitherto unknown proximal TORC1 effector. TORC1-mediated phosphorylation of Vps27 downregulates microautophagy. Thus, vacuolar and endosomal TORC1 balance spatially distinct key regulatory nodes in protein synthesis and degradation, respectively.

## RESULTS

### EGOC Reaches the Vacuolar Surface via the AP-3 Pathway

We previously observed that overproduction of the nucleotide-free Gtr1<sup>S20L</sup> variant strongly inhibited growth in *gtr1Δ* cells through a mechanism that required the TORC1 subunit Tco89

(Binda et al., 2009). This indicates that Rag GTPases can, depending on their nucleotide-binding state, not only activate but also inhibit TORC1. To gain insight into the latter mechanism, we selected suppressor mutations that enabled Gtr1<sup>S20L</sup>-overproducing *gtr1Δ* cells to grow on nutrient-rich medium and mapped the mutations by whole-genome sequencing. Several suppressor mutations (including frameshift mutations and stop codons) were found in genes encoding EGOC subunits (i.e., Ego1, Ego3, and Gtr2), while one mutation affected the Golgi-resident Akr1 that N-terminally palmitoylates Ego1 (Babu et al., 2004; Nadolski and Linder, 2009) (Table 1; Figure S1A). These results indicate that the Gtr1<sup>S20L</sup> allele needs to properly assemble into a membrane-associated EGOC to acquire its capacity to inhibit growth. We also identified one frameshift mutation in *Tco89*, as expected (Binda et al., 2009), as well as a specific point mutation in *TOR1*, which will be studied further elsewhere. Surprisingly, we also mapped 3 mutations in genes that encode subunits of the adaptor protein 3 (AP-3) complex (i.e., Apl6 and Apm3), which functions in cargo-selective protein transport from the TGN to the vacuole (Cowles et al., 1997) and several mutations in genes encoding subunits of the homotypic fusion and vacuole protein sorting (HOPS) complex (i.e., Vam6, Vps41, Vps33, and Vps11), which is required for the fusion of AP-3-coated vesicles with the vacuole (Bowers and Stevens, 2005; Kuhlee et al., 2015). Our independent analysis of individual deletion strains confirmed that loss of any EGOC or HOPS/AP-3 complex subunit (except for Vam6, which plays an additional HOPS complex-independent role in Rag GTPase activation) (Binda et al., 2009) suppressed (to a variable extent) Gtr1<sup>S20L</sup>-mediated growth inhibition (Figure S1B).

Because Ego1 is palmitoylated at the TGN and because the AP-3/HOPS pathway selectively channels cargo from the TGN to the vacuole, our genetic data led us to speculate that Ego1 may travel from the TGN to the vacuole via the AP-3/HOPS pathway. In line with this assumption, loss of the AP-3 subunits Apl5 or Apl6, or of the HOPS complex subunits Vam6 or Vps41 (which also causes vacuoles to fragment), resulted in a partial redistribution of Ego1-GFP from FM4-64-stained vacuoles to the plasma membrane (Figure 1A). Although less apparent at plasma membranes, GFP-Gtr1 was similarly delocalized from vacuolar membranes in AP-3/HOPS complex mutants (Figure 1B). In contrast, localization of GFP-Tor1 to vacuolar membranes and perivacuolar foci remained largely unchanged in the same mutants (Figure 1C). The incomplete dispersal of Ego1 from the vacuole in AP-3 pathway mutants suggested that in these mutants, Ego1 may reach the vacuole through an alternative route such as the carboxypeptidase Y (CPY) pathway that channels proteins from the TGN through the MVB pathway (Bowers and Stevens, 2005). Again, in line with this expectation, combined loss of the AP-3 subunit Apl5 and the t-SNARE Pep12, which is involved in multiple fusion events at the MVB (Bowers and Stevens, 2005), caused Ego1-GFP to mainly localize at the plasma membrane (Figure 1D). Finally, AP-3 adaptors recognize their cargo proteins typically via a dileucine-based sorting signal that is defined by the [D/E]XXXL[L/I] motif (Bonifacino and Traub, 2003). Ego1 harbors an evolutionarily conserved sequence in its N terminus that matches

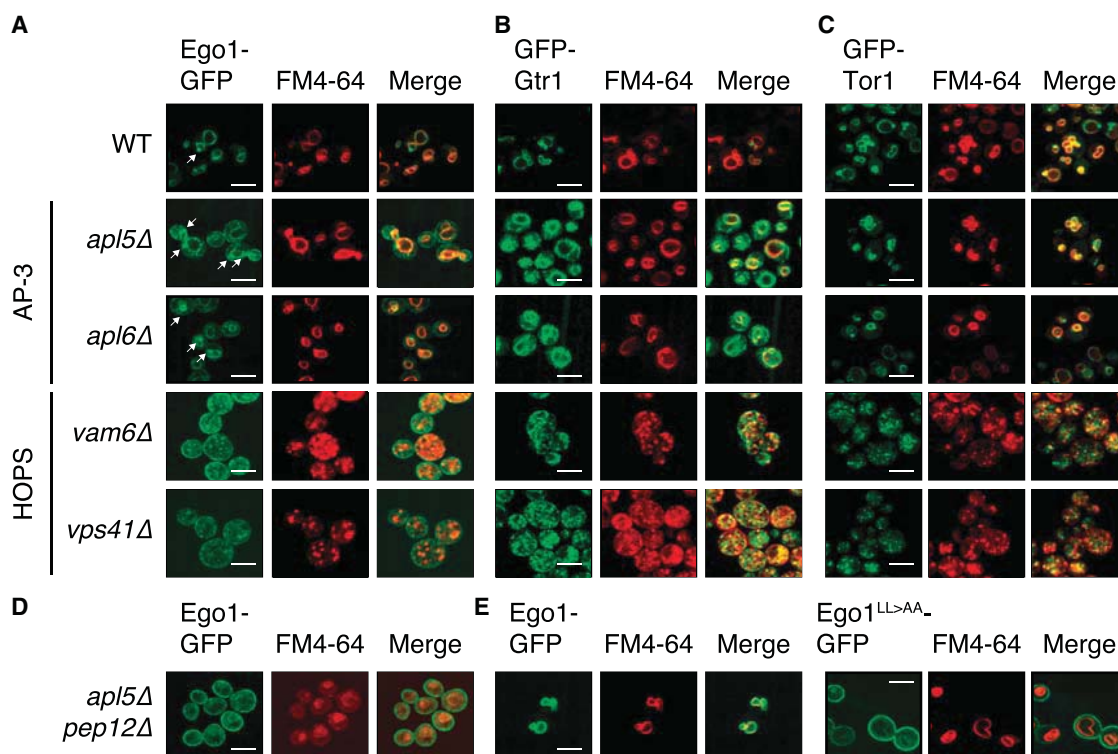


**Figure 1. EGOC, but Not TORC1, Reaches the Vacuolar Surface via the AP-3 Pathway**

(A and B) Genomically tagged Ego1-GFP (A) and GFP-Gtr1 (B) are localized on vacuolar membranes and perivacuolar foci (white arrows) in wild-type (WT) cells but are partially diverted to the plasma membrane and dispersed from the vacuolar membrane, respectively, in AP-3 pathway (*apl5Δ* and *apl6Δ*) and HOPS complex (*vam6Δ* and *vps41Δ*) mutants. Perivacuolar localization of Ego1-GFP was still detectable in AP-3 pathway mutants (A). Moreover, loss of HOPS complex subunits resulted in fragmentation of vacuoles.

(C) AP-3 and HOPS complex function is not required for vacuolar membrane tethering of genomically tagged GFP-Tor1.

(D) Combined loss of Apl5 (AP-3 pathway) and t-SNARE Pep12 (CPY pathway) causes missorting of genomically tagged Ego1-GFP, predominantly to the plasma membrane.

(E) Mutation of the di-leucine motif in Ego1 to di-alanine redirects plasmid-encoded Ego1<sup>L19A/L20A</sup>-GFP (Ego1<sup>LL</sup> > AA-GFP) to the plasma membrane of *ego1Δ* cells.

All strains were grown to exponential phase in synthetic dextrose (SD) medium, stained with the lipophilic styryl dye FM4-64 to visualize vacuolar membranes, and analyzed by fluorescence microscopy. Scale bars, 5 μm (white).

this motif (ENEALL), and mutation of both leucine residues to alanine within this sequence redirected the respective Ego1<sup>LL</sup> > AA-GFP allele predominantly to the plasma membrane (Figure 1E). Thus, our genetic screen uncovered that Ego1, and hence the EGOC, travels from the TGN, where it is palmitoylated, to the vacuolar surface mainly through the AP-3/HOPS complex pathway.

#### Perivacuolar EGOC Foci Embody TORC1-Recruiting Prevacuolar Endosomes

Our data so far provided a rationale for how Ego1 travels from the TGN to the vacuolar membrane. However, they fell short in explaining how Ego1 reaches and clusters in perivacuolar foci: although the high level of vacuole fragmentation in *vam6Δ* and *vps41Δ* cells did not allow us to assess a role of the HOPS complex in directing Ego1-GFP to perivacuolar foci, the AP-3 complex clearly played no role in this process (Figure 1A). We therefore entertained the idea that Ego1 may be routed to perivacuolar foci via the alternative AP-1 or monomeric GGA

(Golgi-localized, γ ear-containing, ARF-binding proteins) adaptors, which have been implicated in cargo transport from the TGN to endosomes (Hanners and Tooze, 2003). We observed that the combined loss of the paralogous Gga1 and Gga2 adaptors, but not loss of the AP-1 subunits Apl2 or Apl4, precluded Ego1-GFP, GFP-Gtr1, and GFP-Tor1 from clustering in perivacuolar foci, while all three proteins were still normally localized at vacuolar membranes in the respective adaptor mutants (Figures 2A–2C). Moreover, we observed that Ego1-GFP, GFP-Gtr1, and GFP-Tor1 all colocalized to a high degree (in >75% of cases for all three proteins, n > 70 each) with Vps21 and Vps27 (Figures 2D–2I), which are reference marker proteins for endosomes that are also termed prevacuolar endosomes (PVEs) in yeast (Day et al., 2018). Conversely, only 47%, 46%, and 54% of Vps27-mCherry-positive endosomes (or PVEs) appeared to contain Ego1-GFP, GFP-Gtr1, and GFP-Tor1, respectively. Thus, EGOC and TORC1 are present on nearly half of the PVEs (which we will refer to simply as endosomes hereafter).

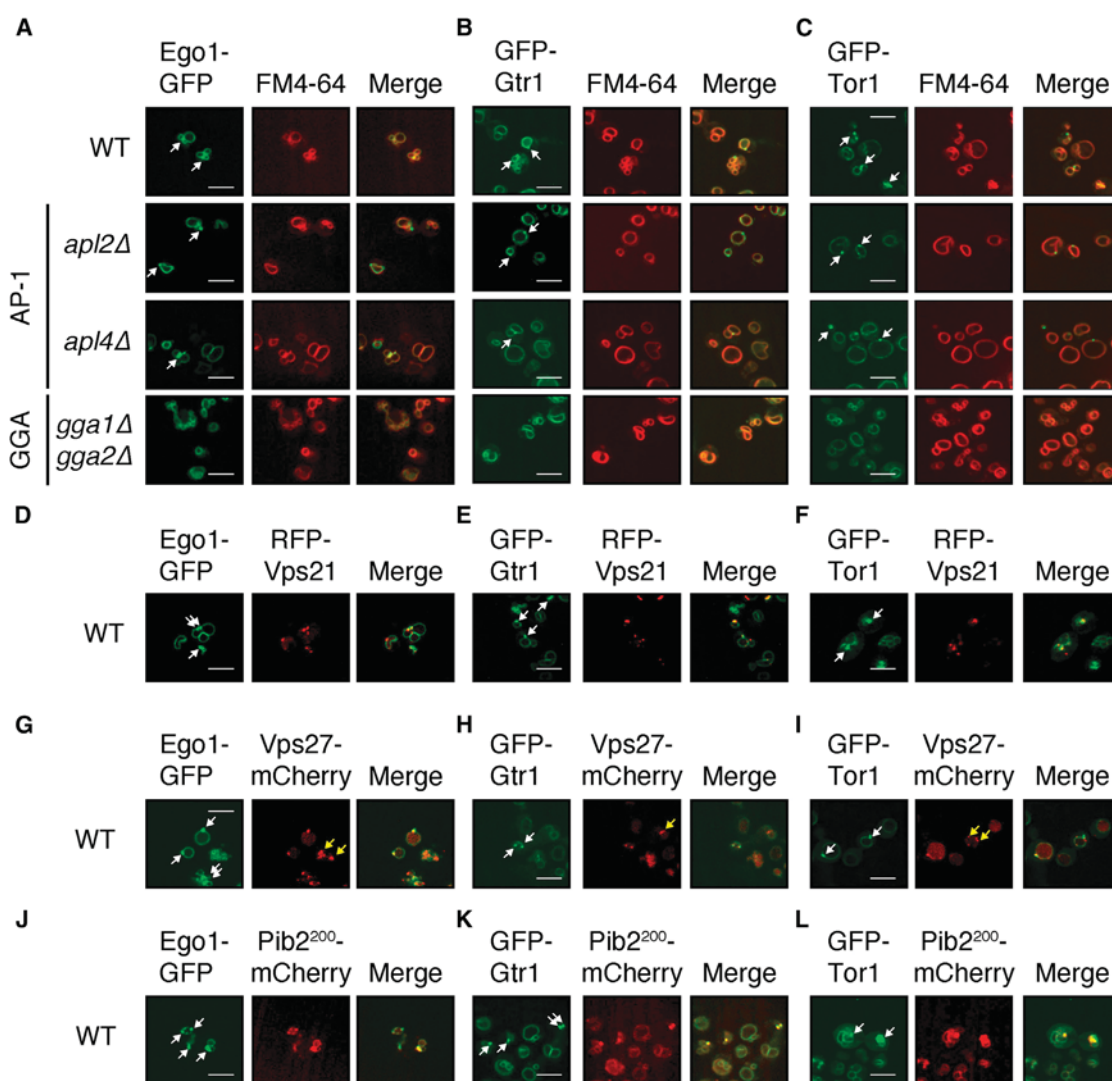


**Figure 2. Perivacuolar EGOC Foci Embody TORC1-Recruiting Prevacuolar Endosomes**

(A–C) Recruitment of genomically tagged Ego1-GFP (A), GFP-Gtr1 (B), and GFP-Tor1 (C) to perivacuolar foci (white arrows) is impaired in the GGA adaptor mutant (*gga1Δ gga2Δ*), but not in the AP-1 pathway mutants (*apl2Δ* and *apl4Δ*).

(D–I) Genomically tagged Ego1-GFP (D and G), GFP-Gtr1 (E and H), and GFP-Tor1 (F and I) colocalize (white arrows) with endosomal marker proteins RFP-Vps21 (D–F, plasmid-expressed) and Vps27-mCherry (G–I, genomically tagged). 53% (*n* = 137), 54% (*n* = 173), and 46% (*n* = 135) of Vps27-mCherry-positive foci appeared to not be matched with Ego1-GFP (G), GFP-Gtr1 (H), and GFP-Tor1 foci (I), respectively (yellow arrows).

(J–L) Genomically tagged Ego1-GFP (J), GFP-Gtr1 (K), and GFP-Tor1 (L) colocalize with Pib2<sup>200</sup>-mCherry at the vacuolar membrane and in perivacuolar foci (white arrows).

All strains were grown to exponential phase in synthetic dextrose medium. Scale bars, 5 μm (white). See also Figure S2.

Our data support a model in which EGOC assembles on endosomes through Ego1, which is escorted from the TGN by its association with the Gga1/2 adaptors. This interaction is likely also mediated by the ENEALL di-leucine motif in Ego1, because it not only matches reasonably well with the canonical GGA-binding motif in mammals (DXLL) (Bonifacino and Traub, 2003) but also is required for Ego1-GFP sorting to both vacuoles and endosomes (Figure 1E). On vacuoles, EGOC teams up with Pib2, a FYVE domain-containing protein that is required for amino acid-mediated activation of TORC1 (Dubouloz et al., 2005; Kim and Cunningham, 2015; Michel et al., 2017; Tanigawa and Maeda,

2017; Varlakhanova et al., 2017), to ensure proper membrane tethering of TORC1 (Ukai et al., 2018). Because Pib2<sup>200</sup>-mCherry almost perfectly colocalized with Ego1-GFP, GFP-Gtr1, and GFP-Tor1 on both vacuoles and endosomes (Figures 2J–2L), we wondered whether the failure of GFP-Tor1 to assemble on endosomes in *gga1/2Δ* cells (Figure 2C) could be explained by the concurrent absence of the EGOC and Pib2 on endosomes of these cells (Ego1 *per se* is not required for this process) (Figure S2E). This seemed to be the case, because both Pib2<sup>200</sup>-mCherry and Ego1-GFP were compromised for their assembly on endosomes in *gga1/2Δ* mutant cells (Figures 2A and S2F).



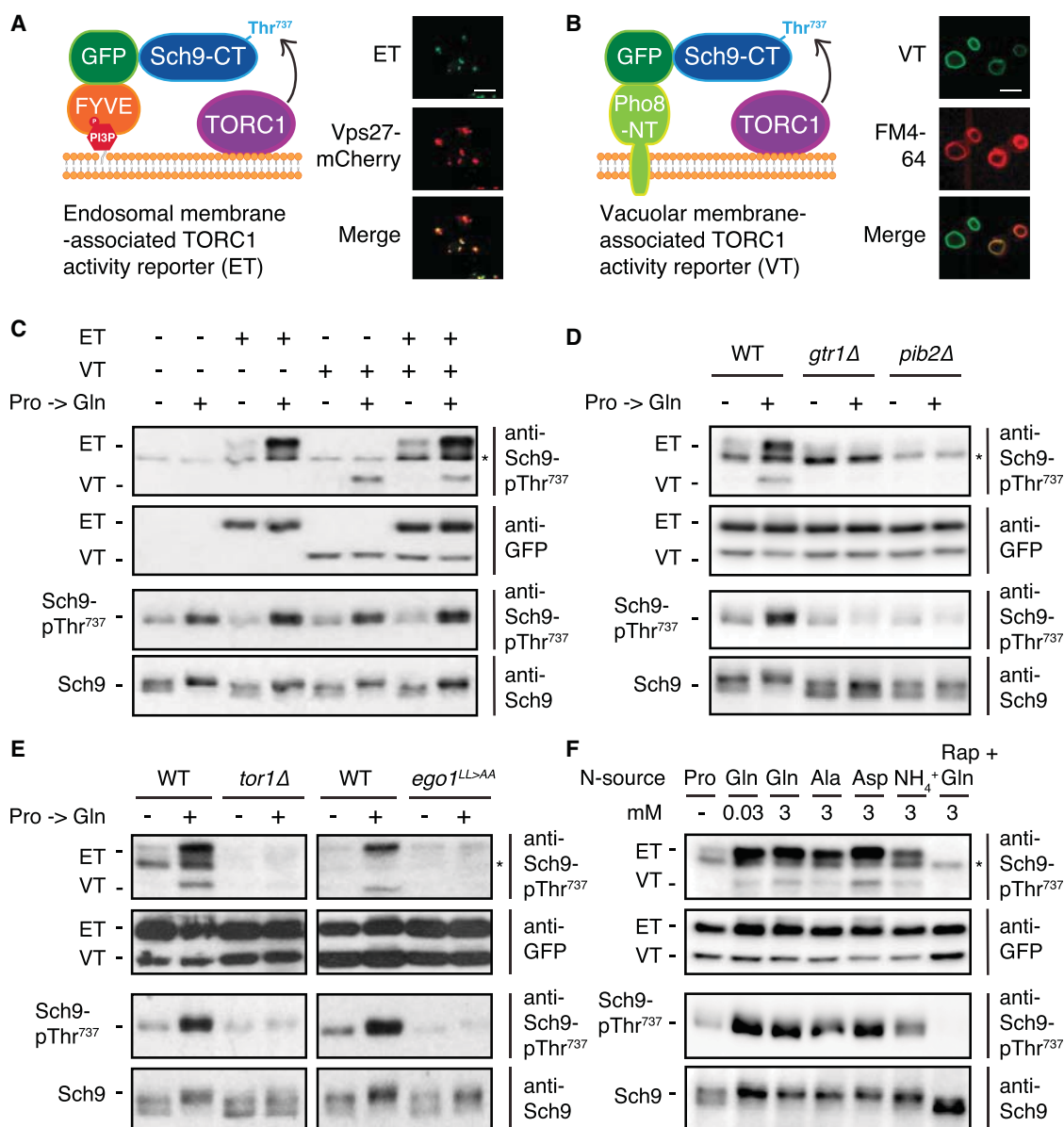


**Figure 3. Mechanistic Control of Endosomal and Vacuolar TORC1 Is Interchangeable**

(A and B) Design of TORC1 activity reporters that specifically probe membrane-associated endosomal TORC1 (ET) or vacuolar TORC1 (VT) TORC1 activity. The ET reporter consists of the EEA1 FYVE domain, which preferentially docks onto PI3P-rich endosomes (Burd and Emr, 1998; Hayakawa et al., 2004), fused to GFP and the C-terminal part of Sch9 that harbors the TORC1 target residue Thr<sup>737</sup> (Urban et al., 2007). In WT cells growing exponentially on synthetic dextrose media containing proline as a nitrogen source (synthetic dextrose-proline), this construct colocalizes with the endosomal marker Vps27-mCherry but is hardly detectable on vacuolar membranes (pictures on the right in A). The VT reporter consists of the C-terminal part of Sch9 fused to GFP and the N-terminal fragment of Pho8. The latter contains an integral membrane segment and directs the entire construct to the vacuolar surface, but not to endosomes (Klionsky and Emr, 1989), as visualized by its colocalization with FM4-64 (pictures on the right in B). Scale bars, 5  $\mu$ m (white).

(C) Both ET and VT reporters are phosphorylated in response to glutamine. WT cells were transformed (+) or not (–) with plasmids expressing ET, VT, or ET and VT reporters combined as indicated; grown to mid-log phase in synthetic dextrose-proline (Pro); and stimulated (+) or not (–) for 2 min with 3 mM glutamine (Gln). The levels of Sch9-pThr<sup>737</sup> on ET and VT reporters (top panel) and on endogenous Sch9 (third panel from the top) were detected by immunoblotting with phosphospecific anti-Sch9-pThr<sup>737</sup> antibodies. Input levels of ET and VT reporters (second panel from the top) or of endogenous Sch9 (bottom panel) were detected with anti-GFP or anti-Sch9 antibodies, respectively. The asterisk denotes a nonspecific signal.

(D) Gtr1 and Pib2 are required for phosphorylation of ET and VT reporters in response to glutamine. Indicated strains were cotransformed with ET and VT reporter-expressing plasmids and analyzed as in (C).

(legend continued on next page)

### Amino Acids Control Both Endosomal and Vacuolar TORC1

To evaluate a model in which TORC1 functions in spatially separated pools, we designed specific reporters that allowed us to independently assess endosomal TORC1 (ET) and vacuolar TORC1 (VT) activities as illustrated in Figures 3A and 3B. In cells grown in media containing the poor nitrogen source proline, the phosphorylation level of Sch9-Thr<sup>737</sup> on both ET and VT reporters was similar to the one on endogenous Sch9 (Figure 3C), very low. Glutamine stimulation, however, strongly increased the phosphorylation level of this residue on both reporters and on endogenous Sch9 (Figure 3C), which supports the existence of amino acid-responsive TORC1 on both endosomes and vacuoles. We next sought to evaluate whether these pools of TORC1 may be discriminated by differential modes of amino acid-mediated activation. The respective experiments revealed that both ET and VT required the presence of Gtr1 and Pib2 to be properly activated by glutamine addition (Figure 3D), which was not surprising given the strikingly comparable distribution of Gtr1 and Pib2 within cells (Figure 2K). Similarly, *tor1Δ* cells, or *ego1Δ* cells expressing the di-leucine mutant Ego1<sup>LL > AA</sup> that is unable to assemble endosomal and vacuolar EGOs (Figure 1E), were compromised in their ability to activate both ET and VT in response to glutamine addition (Figure 3E). Finally, both pools of TORC1 responded analogously to quantitative (i.e., 0.03 and 0.3 mM glutamine) or qualitative (i.e., strong or weaker activation by glutamine and aspartate or alanine and NH<sub>4</sub><sup>+</sup>, respectively) variations of the added nitrogen source and were equally sensitive to rapamycin treatment (Figure 3F). Thus, ET and VT are subjected to amino acid-dependent control mechanisms that appear interchangeable.

### ET and VT Pools Are Functionally Autonomous

Having established the existence of spatially distinct TORC1 assemblies, we next wondered whether this observation bears any functional relevance. To address this issue, we first tried to uncouple the regulation of ET and VT by different means. One way to achieve this might be through deletion of the genes encoding subunit a of the endosomal (Stv1) or vacuolar (Vph1) V-ATPases (Forgac, 2007), which we anticipated may activate TORC1 similar to fly and mammalian V-ATPases that mediate amino acid signals through Ragulator and RAGA/B (Zoncu et al., 2011). Gratifyingly, loss of Vph1 abolished the glutamine-mediated phosphorylation of the VT but only mildly affected the respective phosphorylation of the ET reporter (both reporters localized as expected in all mutants analyzed) (Figures 4A, 4B, and S3A). Thus, only Vph1-containing V-ATPases act upstream of VT, which is substantiated by our observation that loss of Vph1 significantly reduced the glutamine-mediated phosphorylation of Sch9, the proposed target of TORC1 at the vacuole (Jin et al., 2014). Loss of Stv1, in contrast, affected neither ET nor VT unless it was combined with loss of Vph1, in which case

both ET and VT were unable to respond to glutamine addition (Figure 4A). Stv1- and Vph1-containing V-ATPases therefore function analogously and redundantly in amino acid-dependent activation of ET, which matches well with Vph1-containing V-ATPases transiting through endosomes *en route* to the vacuole (Forgac, 2007).

Altogether, our analysis of V-ATPase mutants revealed that ET can function independently of and in the absence of VT (in *vph1Δ* cells), yet it did not allow us to establish an inverse situation in which only ET was abrogated. In this context, we were intrigued by a study of an internally GFP-tagged Tor1<sup>D330</sup>-3GFP allele (originally created by Sturgill et al., 2008), which failed to oligomerize VT complexes into TOROIDs (TORC1 organized in inhibited domains) in glucose-starved cells and appeared to be less competent in associating with perivacuolar foci in exponentially growing cells (Prouteau et al., 2017). A closer analysis of the latter phenotype in exponentially growing cells confirmed that Tor1<sup>D330</sup>-3GFP was able to reach vacuolar membranes but was rarely present in perivacuolar foci (Figure 4C). In line with these cell biological data, expression of the Tor1<sup>D330</sup>-3GFP allele enabled us to establish a condition in which cells were significantly compromised for their ability to phosphorylate the ET but not the VT reporter in response to glutamine addition (Figure 4D). Conversely, we were able to specifically restore ET, but not VT, in exponentially growing and glutamine-stimulated *tor1Δ* cells by expressing a hyperactive, mCherry-tagged Tor1<sup>I1954V</sup> allele (Reinke et al., 2006), which was targeted to endosomes via an N-terminally fused FYVE domain (Figures 4E and S3). Finally, loss of Tco89 caused GFP-Tor1 to disperse from vacuolar membranes and to cluster on Vps27-mCherry-positive endosomes (Figure 4F), which was accompanied by an increase in ET activity in cells growing exponentially on proline-containing medium (Figures 4G and 4H). Although Tco89 was required for glutamine-mediated activation of both ET and VT (Figures 4G and 4H), these experiments show that ET and VT activities can be uncoupled from each other and corroborate a model in which both pools of TORC1 are functionally autonomous.

### ET Targets ESCRT-0

The existence of a distinct endosomal pool of TORC1 advocates a model in which specific biological processes that emanate from endosomes may need to be wired to the nutritional status of the cell. One such process may involve the partitioning of the Vps27-Hse1 ESCRT-0 machinery between the MVB pathway on endosomes, where Vps27 seemed to colocalize with EGO and TORC1 in well-fed cells (Figures 2G–2I), and the identified ESCRT-dependent microautophagic process that takes place on vacuoles in nutrient-starved cells (Oku et al., 2017; Zhu et al., 2017). To experimentally address this idea, we first asked whether Vps27 (a composite structural model of which is shown in Figure 5A) could be a substrate of TORC1 *in vitro*. These

(E) Loss of Tor1 or expression of Ego1<sup>L19A/L20A</sup>-GFP abolishes glutamine-mediated activation of both ET and VT. WT and *tor1Δ* cells (left panels) or *ego1Δ* cells expressing ET and VT reporters, together with Ego1-GFP (WT) or Ego1<sup>L19A/L20A</sup>-GFP (*ego1<sup>LL > AA</sup>*) from plasmids (right panels), were analyzed as in (C).

(F) Both ET and VT reporters respond similarly to various nitrogen sources. WT strains coexpressing ET and VT reporters were analyzed as in (C), except that they were stimulated for 2 min with the indicated concentrations of glutamine (Gln), alanine (Ala), aspartate (Asp), or NH<sub>4</sub><sup>+</sup>. Rapamycin (200 ng mL<sup>-1</sup>; applied 30 min before Gln addition) abolished Gln-mediated phosphorylation of ET and VT reporters and of endogenous Sch9.

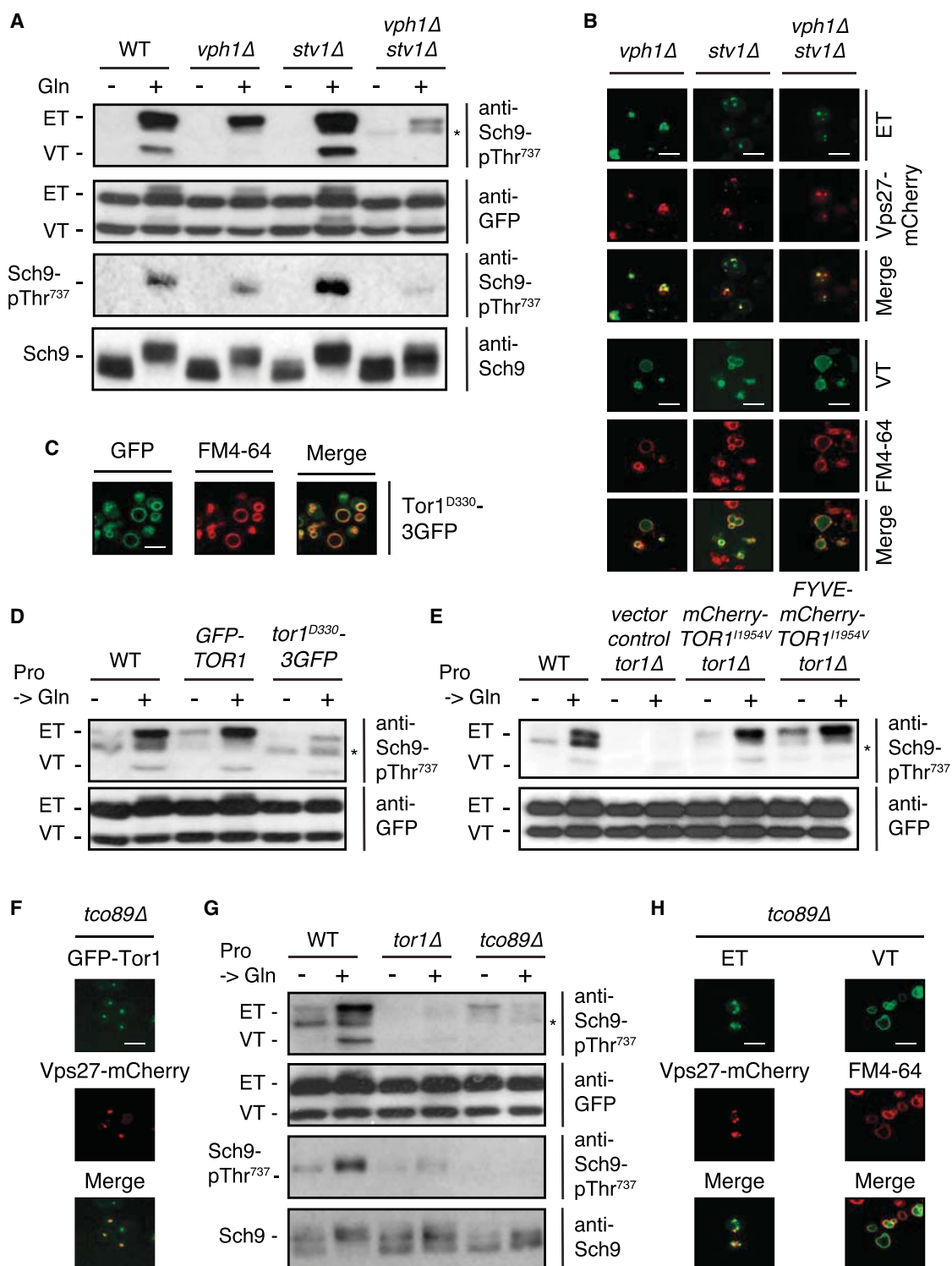


**Figure 4. ET and VT Are Functionally Autonomous**

(A and B) Vph1, the a subunit of vacuolar V-ATPase, is specifically required for glutamine-mediated activation of VT, while activation of ET requires either Vph1 or Stv1, the a subunit of endosomal V-ATPase. Indicated strains expressing ET and VT reporters were grown to mid-log phase in synthetic dextrose medium buffered at pH 6.0. For nitrogen starvation (–), cells were filtered, washed, resuspended in synthetic dextrose-N medium buffered at pH 6.0, and incubated for 30 min. Starved cells (–) were then restimulated for 2 min with 3 mM glutamine (+) and analyzed as in Figure 3C (A). In control experiments, ET and VT reporters were colocalized in the indicated strains with Vps27-mCherry and FM4-64, respectively (B). Scale bars, 5 μm (white). See also Figure S3A.

(legend continued on next page)

analyses revealed that TORC1 (purified from yeast) phosphorylated recombinant Vps27 (copurified with Hse1) in the absence, but not in the presence, of the ATP-competitive TOR inhibitor Torin2 (Liu et al., 2013) (Figure 5B). Mass spectrometry analyses of Vps27 proteins that were subjected to *in vitro* TORC1 kinase assays allowed us to identify 5 phosphopeptides harboring 10 potential phospho-serine (Ser) or threonine (Thr) residues (Table S1), which all localize to apparently unstructured loops within Vps27 (Figure 5A). Because TORC1 was unable to phosphorylate *in vitro* a recombinant Vps27<sup>10A</sup> variant in which all 10 Ser or Thr residues were substituted with alanine (Ala) (Figure 5B), we inferred that these 10 residues encompass most residues in Vps27 that are modified by TORC1. To assess whether TORC1 may also phosphorylate Vps27 *in vivo*, we performed quantitative phosphoproteomic analyses by stable isotope labeling by amino acids in cell culture (SILAC) (Ong et al., 2002) using extracts from cycloheximide-treated and untreated yeast cells. Addition of cycloheximide activates TORC1, as was shown by increased phosphorylation of Sch9 (Binda et al., 2009; Urban et al., 2007). These assays retrieved the same 5 Vps27 phosphopeptides that we obtained in our *in vitro* assays and allowed us to pinpoint unequivocally 7 residues, of which minimally 2, Ser<sup>155</sup> and Thr<sup>159</sup>, seemed to be regulated by TORC1 *in vivo* (Figure S4). To corroborate our *in vivo* data, we analyzed the *in vivo* phosphorylation pattern of Vps27 by Phos-tag gel electrophoresis. Vps27 from extracts of exponentially growing cells separated into four distinct bands, of which the slowest migrating one was faint (Figure 5C). Addition of cycloheximide significantly increased the intensity of the two upper, slowly migrating hyperphosphorylated forms of Vps27 (at the expense of the two faster migrating bands), and this effect was largely blocked in the presence of rapamycin (Figure 5C). In addition, hyperphosphorylation of Vps27 was mediated by ET, because the expression of FYVE-Tor1<sup>I1954V</sup> in *tor1Δ* cells, which have high ET and low VT activity (Figure 4E), specifically boosted the levels of the slowest migrating Vps27 isoform (Figure 5D); conversely, in cells expressing Tor1<sup>D330</sup>-3GFP, which have low ET and normal VT activity (Figure 4D), the latter Vps27 isoform was absent and the two hypophosphorylated, slowly migrating isoforms were most prominent (Figure 5E). Finally, a Vps27<sup>10D</sup> variant in which all 10 putative TORC1 target residues were substituted with aspartates (Asp; D) migrated under all conditions tested within two discrete bands (of which one may correspond to a variant that is phosphorylated at Ser<sup>613</sup> by Pkh1/2 (Morvan et al., 2012) (Figure 5C). Altogether, these data establish Vps27 as a direct target of ET within cells.

To study the role of TORC1-mediated phosphorylation of Vps27 *in vivo*, we needed to identify a Vps27-dependent process

that was modulated by TORC1 activity. As outlined earlier, we reasoned that microautophagy of vacuolar membrane proteins may be a prime candidate process that meets this requirement. This was the case, because rapamycin treatment induced the degradation of the GFP-tagged vacuolar membrane protein Pho8 (visualized by the accumulation of the cleaved, stable GFP moiety) and this depended on Vps27 (Figure 5F). To mimic the TORC1-phosphorylated state of Vps27, we mutated (in various combinations) the 10 presumed TORC1 target sites to Asp and analyzed the properties of the different Vps27 alleles *in vivo*. Two sets of mutations in Vps27 (i.e., S155D, S157D, and T159D, as well as S174D, S177D, S179D, and S280D) significantly reduced the rapamycin-induced degradation of GFP-Pho8 (Figure S5). Expression of a Vps27 allele that combined all 7 mutations (Vps27<sup>7D</sup>) was slightly more defective in the same assay (Figure 5F), suggesting that TORC1 inhibits ESCRT-driven microautophagy mainly via phosphorylation of these 7 residues in Vps27. To gain further insight into this process, we asked whether TORC1 affects the subcellular localization of Vps27. The respective studies revealed that both wild-type pHluorin-Vps27 and pHluorin-Vps27<sup>7D</sup> localized predominantly on endosomes and were barely detectable on vacuolar membranes in exponentially growing cells (Figure 5G). However, rapamycin treatment did not visibly change the localization pattern of Vps27 or of Vps27<sup>7D</sup>, although we expected at least a minor part of Vps27 to cluster at vacuolar membranes, where it initiates microautophagy under these conditions. We therefore deemed it possible that Vps27 only briefly stops over on vacuolar membranes to bind cargo proteins and then travels conjointly with these into microautophagic vesicles for subsequent degradation. In line with this assumption, rapamycin treatment triggered a partial degradation of pHluorin-Vps27, like the one of GFP-Pho8 (Oku et al., 2017), in a manner that depended on the presence of the vacuolar protease Pep4 (Figure 5H). Because Vps27 docks to ubiquitinated cargo on membranes through the combined action of its ubiquitin-binding (ubiquitin-interacting motif 1/2 [UIM1/2]) and PI3P-binding (FYVE) domains (Figure 5A) (Henne et al., 2011), our data are most simply explained in a model in which TORC1-mediated phosphorylation of Vps27 on endosomes results in structural changes on Vps27 that diminish its overall affinity for cargo on vacuolar membranes that contain, unlike endosomes, low levels of PI3P (Marat and Haucke, 2016). This fits well with our observation that the phosphomimetic Vps27<sup>7D</sup> variant was more resistant to degradation than wild-type Vps27 before and during the 3-hr treatment with rapamycin (Figure 5H). A more fine-grained model of the effects of the respective phosphorylation events will require detailed structural and biochemical analyses of the interaction

(C) Genomically tagged Tor1<sup>D330</sup>-3GFP localizes normally on vacuolar membranes (stained with FM4-64) but is largely unable to assemble on perivacuolar foci (for comparison, see GFP-Tor1 depicted in Figures 1C and 2C). Scale bar, 5 μm (white).

(D) Expression of genomically tagged Tor1<sup>D330</sup>-3GFP, but not that of GFP-Tor1, compromises the capacity of exponentially growing cells to sustain normal levels of ET activity and to activate it in response to glutamine addition. For details, see Figure 3C.

(E) Expression of FYVE-mCherry-Tor1<sup>I1954V</sup> stimulates ET, but not VT, in exponentially growing and glutamine-treated *tor1Δ* cells. Control cells carried an empty vector, or expressed plasmid-encoded mCherry-Tor1<sup>I1954V</sup>, which supports both ET and VT activity. For details, see Figure 3C. See also Figure S3B.

(F–H) Loss of Tco89 causes accumulation of GFP-Tor1 on Vps27-mCherry-positive endosomes (F), stimulates ET specifically in exponentially growing cells (F), and abolishes glutamine-mediated activation of ET and VT (G). Controls include WT cells and *tor1Δ* cells that are defective in ET and VT reporter phosphorylation. For details, see Figures 3C and 3E. ET and VT reporters colocalized in the *tco89Δ* cells with Vps27-mCherry and FM4-64, respectively (H). Scale bars, 5 μm (white).



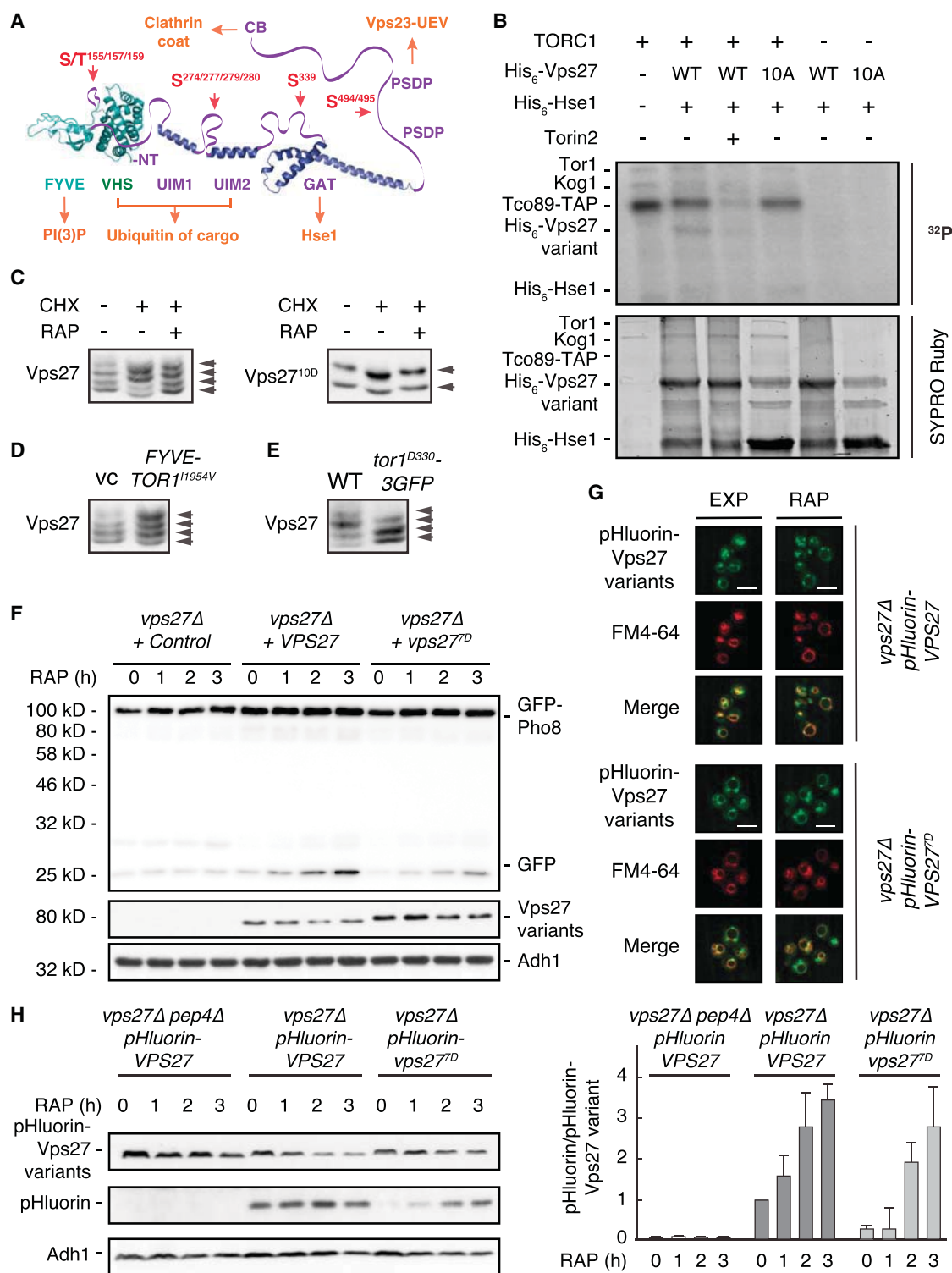


**Figure 5. ET Targets Vps27**

(A) Composite model of Vps27. The various structural domains of Vps27 were assembled as in Hurley et al. (2009) and include the PI3P-binding FYVE domain, the VHS (Vps27, Hrs, STAM) and UIM1/2 (ubiquitin-interacting motif) domains that cooperate in binding polyubiquitinated cargo, the GAT (GGA and TOM1 homology) domain that mediates heterodimerization with Hse1, the PSDP motifs that recruit the ESCRT-I protein Vps23 via its N-terminal ubiquitin-conjugating enzyme E2 variant (UEV) domain, and the C-terminal clathrin-binding (CB) motif. Serine (S) and threonine (T) residues that are targeted by TORC1 *in vitro* (see B) are highlighted in red. See also Table S1.

(legend continued on next page)

of Vps27 variants with cargo proteins on membranes of different composition.

### ET Targets Atg13

Atg13 is an essential regulatory element of macroautophagy and a well-established target of TORC1 in yeast (Kamada et al., 2010). In exponentially growing cells, Atg13 is localized diffusely in the cytoplasm, but upon nitrogen starvation and/or TORC1 inhibition, it nucleates autophagosome production from defined perivacuolar foci called preautophagosomal structures (PASs) (Suzuki et al., 2001, 2013). Because TORC1-mediated phosphorylation of Atg13 terminates the latter process (Kamada et al., 2010), ET may be predestined to fulfill this task if it were close to the PASs. We observed that both Atg13-mCherry and Atg13-GFP were localized in the cytoplasm in exponentially growing cells as expected; to our surprise, however, these Atg13 variants localized close to and/or even colocalized with endosomal GFP-Tor1 or GFP-Gtr1 in nitrogen-starved cells (Figures 6A and 6B). In addition, Atg13 was dispersed from these foci as expected upon readdition of glutamine to nitrogen-starved cells (Figures 6A and 6B). The latter effect was paralleled by a swift hyperphosphorylation of Atg13 that depended strongly on ET, because it was observed to a greater extent in FYVE-mCherry-Tor1<sup>I1954V</sup>- and mCherry-Tor1<sup>I1954V</sup>-expressing *tor1Δ* cells than in *tor1Δ* control cells (Figure 6C). Conversely, Tor1<sup>D330</sup>-3GFP-expressing cells with low ET activity were clearly defective for Atg13 hyperphosphorylation (but not for Sch9-Thr<sup>737</sup> phosphorylation) when compared to isogenic wild-type cells (Figure 6D). These observed differences in glutamine-mediated Atg13 hyperphosphorylation were mirrored by the relative speed by which the PASs were dispersed in the respective cells. Accordingly, PASs were more rapidly disassembled in glutamine-refed FYVE-mCherry-Tor1<sup>I1954V</sup>- or mCherry-Tor1<sup>I1954V</sup>-expressing *tor1Δ* cells than in *tor1Δ* control cells or in Tor1<sup>D330</sup>-3GFP-ex-

pressing cells (Figure 6E). Thus, ET appears to be specifically commissioned to control macroautophagy via Atg13.

### DISCUSSION

Studies in different organisms have shown that TORC1 is abundantly localized on vacuolar and lysosomal membranes from which it centrally controls many aspects of cell growth under nutrient-rich conditions (Betz and Hall, 2013). Conceivably, however, the precise spatial and temporal control of growth requires TORC1 to control targets within subcellular neighborhoods other than the vacuole and lysosome. In line with this reasoning, mammalian cells have been found to express two perhaps structurally divergent TORC1 complexes that signal separately from the lysosome or the Golgi compartment to preferentially control S6K or the eukaryotic translation initiation factor 4E-binding protein (4E-BP), respectively (Fan et al., 2016). However, other examples for a spatially sequestered division of labor between populations of TORC1 have remained largely elusive. Here, we show that yeast TORC1, in addition to controlling protein synthesis via its vacuolar target Sch9 (Jin et al., 2014; Takeda et al., 2018; Urban et al., 2007), specifically regulates Vps27 and Atg13 on PVEs to fine-tune micro- and macroautophagy, respectively (Figure 6F). Regulation of Vps27 and Atg13 at the level of endosomes appears to be judicious, because both proteins operate, at or proximal to endosomes, as gatekeepers of the specific autophagic processes. Vps27, for instance, predominantly localizes on endosomes, where it plays a key role in MVB sorting in nutrient-fed cells (Henne et al., 2011). ET is therefore ideally placed to maintain this function and prevent the unscheduled deployment of Vps27 to the vacuolar surface, where it executes its alternative task in microautophagy in starvation conditions (Oku et al., 2017; Zhu et al., 2017). In contrast, Atg13 aggregates within endosome-proximal structures called PASs in nutrient-starved cells with low TORC1 activity, which

(B) TORC1 phosphorylates Vps27 *in vitro*. Recombinant His<sub>6</sub>-Vps27 (WT) and His<sub>6</sub>-Vps27<sup>10A</sup> (10A), in which all 10 serine or threonine residues highlighted in (A) were mutated to alanine residues, were copurified with His<sub>6</sub>-Hse1 and subjected to *in vitro* phosphorylation by TORC1 (purified from yeast) in the absence (–) or presence (+) of the TOR inhibitor Torin2. Representative SYPRO Ruby staining and autoradiography (<sup>32</sup>P) blots are shown.

(C) Vps27 phosphorylation is regulated by TORC1 *in vivo*. *vps27Δ* cells expressing Vps27 or Vps27<sup>10D</sup> from plasmids were grown to exponential phase on synthetic dextrose. They were either left untreated (–) or treated with cycloheximide (CHX, 25 μg mL<sup>–1</sup>; +) for 30 min with (+) or without (–) prior addition of rapamycin (RAP, 200 ng mL<sup>–1</sup>; +) for 30 min. Phosphorylation of the Vps27 variants was analyzed on a Phos-tag gel followed by immunoblotting with anti-Vps27 antibodies. Arrowheads indicate phosphoisoforms. See also Figure S4.

(D) ET targets Vps27. *tor1Δ* cells expressing or not expressing (vector control [vc]) FYVE-mCherry-Tor1<sup>I1954V</sup>, together with plasmid-encoded Vps27, were grown exponentially in synthetic dextrose and analyzed as in (C).

(E) Tor1<sup>D330</sup>-3GFP-expressing cells exhibit lower Vps27 phosphorylation levels when compared to WT cells. Cells were grown and analyzed as in (D).

(F) TORC1 impinges on Vps27 to inhibit ESCRT-driven degradation of vacuolar membrane-resident GFP-Pho8. Cells expressing or not expressing (control) indicated plasmid-encoded Vps27 variants were grown exponentially (0), treated with rapamycin (200 ng mL<sup>–1</sup>) for the times indicated, and subjected to immunoblot analyses (using anti-GFP antibodies) to measure the levels of GFP cleavage from plasmid-expressed GFP-Pho8. The serine residues 155, 157, 274, 277, 279, and 280 and the threonine residue 159 of Vps27 were mutated to phosphomimetic aspartates to yield the Vps27<sup>7D</sup> allele. The levels of Vps27 and Vps27<sup>7D</sup> were analyzed by immunoblot analysis using anti-Vps27 antibodies. Adh1 levels served as loading controls. See also Figure S5.

(G) TORC1 phosphorylation sites on Vps27 do not visibly control its partitioning between endosomes and vacuoles. FM4-64-stained *vps27Δ* cells expressing pHluorin-Vps27 or pHluorin-Vps27<sup>7D</sup> were grown exponentially in synthetic dextrose (EXP), treated with rapamycin (RAP; 200 ng mL<sup>–1</sup>; 2 hr), and analyzed by fluorescence microscopy. Scale bars, 5 μm (white).

(H) Inhibition of TORC1 induces Pep4-dependent degradation of pHluorin-Vps27. pHluorin-Vps27-expressing *vps27Δ* and *vps27Δ pep4Δ* cells, along with pHluorin-Vps27<sup>7D</sup>-expressing *vps27Δ* cells, were grown in synthetic dextrose and treated as in (F). The levels of full-length pHluorin-Vps27 variants and released pHluorin were assessed by immunoblot analysis using anti-GFP antibodies and classical and Radiance Plus-sensitive enhanced chemiluminescence (ECL), respectively (because the relative amount of cleaved pHluorin versus full-length pHluorin-Vps27/-Vps27<sup>7D</sup> was lower than 5% in each sample). Adh1 levels served as loading controls. Representative immunoblots are shown. Degradation of pHluorin-Vps27 variants was estimated as the ratio between released pHluorin and full-length pHluorin-Vps27 alleles throughout the rapamycin treatment. Values were normalized to the one for pHluorin-Vps27-expressing *vps27Δ* cells at time 0 and presented in the bar graph as means (n = 3; ±SD).

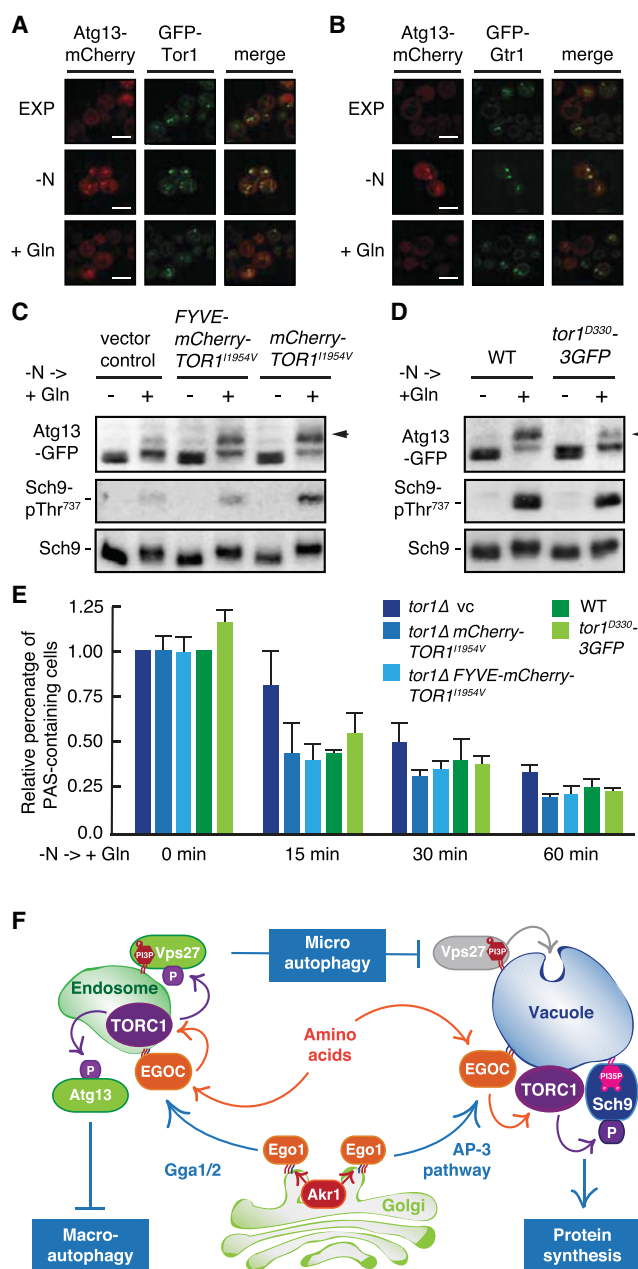


**Figure 6. ET Targets Atg13**

(A and B) Atg13 localizes close to endosomal Tor1 and Gtr1 in nitrogen-starved cells. Cells coexpressing Atg13-mCherry and either GFP-Tor1 (A) or GFP-Gtr1 (B) were grown exponentially in synthetic dextrose medium (EXP), starved for nitrogen (60 min; -N), restimulated with 3 mM glutamine (60 min; +Gln), and analyzed by fluorescence microscopy. Scale bars, 5  $\mu$ m (white).

(C) ET targets Atg13. *tor1*Δ cells expressing or not expressing (vector control) mCherry-Tor1<sup>11954V</sup> or FYVE-mCherry-Tor1<sup>11954V</sup> from plasmids were grown exponentially on synthetic dextrose, starved for nitrogen (60 min; -N; -), and restimulated with 3 mM glutamine (2 min; +Gln; +). Phosphorylation of Atg13-GFP was analyzed by immunoblotting with anti-GFP antibodies. The arrow indicates the hyperphosphorylated Atg13 isoforms. The levels of endogenous Sch9-pThr<sup>737</sup> (middle panel) and of Sch9 (bottom panel) were probed as in Figure 3C. Strains with compromised VT (i.e., *tor1*Δ and *tor1*Δ FYVE-mCherry-TOR1<sup>11954V</sup>) are, unlike mCherry-Tor1<sup>11954V</sup>-expressing strains, defective for normal Sch9 phosphorylation upon glutamine restimulation.

is somewhat reminiscent of the situation in mammalian cells, where autophagosome assembly sites develop from recycling endosomes (Puri et al., 2018). In this case, ET is perfectly placed to disassemble and disperse the supramolecular macroautophagy initiation complexes of the PASs through phosphorylation of Atg13 (Yamamoto et al., 2016), specifically when nutrients become available again. Thus, TORC1 elegantly coordinates micro- and macroautophagy by controlling the phosphorylation state of Vps27 and Atg13 at or near endosomes.

TORC1 foci that form in exponentially growing cells have been described before, but it has remained unclear whether they represent independent subcellular structures or were shaped by aggregation of TORC1 on the vacuolar surface (Binda et al., 2009; Kira et al., 2016; Varlakhanova et al., 2017). The latter type of foci exist, but they emerge specifically in glucose-starved cells (not in nitrogen-starved cells), where they inhibit TORC1 within higher-level assemblies called TOROIDs downstream of the Gtr1/Gtr2 nucleotide-loading status (Prouteau et al., 2017). The TORC1 foci described here, in contrast, are discernible in exponentially growing cells, where they correspond to active TORC1 on perivacuolar endosomes. The latter have been described as long-lived compartments of stable composition that deliver intraluminal vesicles by “kiss-and-run” events to the proximal vacuole (Day et al., 2018). This might allow partial redistribution of membrane resident and attached proteins between both compartments. It is therefore not surprising that the distribution of TORC1 between endosomes (or perivacuolar foci) and vacuoles remains largely unaffected by nitrogen or amino acid starvation and is only mildly affected by the nucleotide-binding state of the Rag GTPases (Binda et al., 2009; Kira et al., 2014, 2016; Varlakhanova et al., 2017). At variance with these observations, however, one study posits that nitrogen starvation strongly influences this distribution, although it remains unclear whether the respective cells were truly nitrogen starved, because they were shifted from a complete medium (supplemented with adenine and uracil) to a different medium called YMM (Ukai et al., 2018). Because the surface landscapes of endosome and vacuoles are different and may even be structured individually by the action of TORC1, it is in theory possible that specific nutritional fluctuations temporally shift the overall dissemination of TORC1 between these compartments.

(D) *tor1*<sup>D330-3GFP</sup>-expressing cells are defective for Atg13 phosphorylation upon glutamine refeeding to nitrogen-starved cells. Wild-type and *tor1*<sup>D330-3GFP</sup> cells expressing genomically tagged Atg13-GFP were grown and analyzed as in (C).

(E) ET controls PAS dispersal. Cells (as in C, blue bars, or WT and isogenic *tor1*<sup>D330-3GFP</sup> cells coexpressing Atg13-mCherry, green bars) were grown as in (C) and (D) and analyzed for the dispersal of PASs (Atg13-GFP or Atg13-mCherry foci) following glutamine refeeding for the times indicated. Bars denote the percentage of PAS-containing cells ( $n = 3$ ;  $\pm$ SD) normalized to the *tor1*Δ vector control strain (in which 83.1% of the cells exhibit a PAS; blue bars) or the WT strain (in which 67.9% of the cells exhibit a PAS; green bars) following the 60-min nitrogen starvation period (0 min). More than 75 cells were counted at each time point.

(F) Spatially distinct pools of EGOC and TORC1 control microautophagy, macroautophagy, and protein synthesis. Arrows and bars denote positive and negative interactions, respectively. P, phosphorylated residues. For details, see text.

The discovery of spatially separated pools of TORC1 that target their own set of effectors also requires critical reconsideration of previous conclusions from studies in which TORC1 foci formation was correlated with VT activity (Kira et al., 2016; Ukai et al., 2018). For instance, loss of Tco89 causes TORC1 to disperse from vacuoles and to cluster in foci (Varlakhanova et al., 2017), which we identify here as endosomes (Figure 4F). The clustering of TORC1 on endosomes correlates with very low TORC1 activity when using Sch9 phosphorylation as readout and could hence be interpreted as TORC1 being inactive on endosomes. This is, however, not the case, because ET (assayed via our ET reporter) is, although unresponsive to glutamine addition, hyperactive in exponentially growing *tco89Δ* cells (Figures 4G and 4H). Our data not only clarify earlier published conflicting data and their interpretations but also pinpoint an intriguing model in which ET and VT complexes may be structurally and functionally divergent, which is also supported by our finding that Tor1<sup>D330</sup>-3GFP assembles functional TORC1 complexes at the vacuole, but not on endosomes. Future studies are therefore warranted that address the questions whether such disparities exist and whether they may be explained with the divergent surface composition of endosomes and vacuoles. In a similar vein, it will be interesting to evaluate whether the metabolic content of and regulatory elements on endosomes and vacuoles may differentially feed into the TORC1 pathway.

## STAR★METHODS

Detailed methods are provided in the online version of this paper and include the following:

- KEY RESOURCES TABLE
- CONTACT FOR REAGENT AND RESOURCE SHARING
- EXPERIMENTAL MODEL AND SUBJECT DETAILS
- METHOD DETAILS
  - Yeast Strains, Plasmids, and Growth Conditions
  - Whole Genome Sequencing
  - Fluorescence Microscopy
  - Cell Lysate Preparation and Immunoblot Analyses
  - Phos-tag Gel Analysis of Vps27 Isoforms
  - Purification of Recombinant Vps27-Hse1 Complexes
  - TORC1 Purification
  - *In Vitro* TORC1 Kinase Assays
  - *In Vivo* TORC1 Kinase Assays
  - Filter-Aided *In Vitro* Kinase Assay and Phosphopeptide Enrichment
  - Sample Preparation of *In Vivo* SILAC Experiments
  - Mass Spectrometry Analyses
- QUANTIFICATION AND STATISTICAL ANALYSIS
- DATA AND SOFTWARE AVAILABILITY

## SUPPLEMENTAL INFORMATION

Supplemental Information includes five figures and one table and can be found with this article online at <https://doi.org/10.1016/j.molcel.2018.10.040>.

## ACKNOWLEDGMENTS

We thank Laurent Falquet for the bioinformatic analyses of the whole genome sequences, Benjamin Pillet for help with assembling Figure 5A, and Yoshinori

Ohsumi, Takeshi Noda, Scott Emr, Robbie Loewith, and BIOS ToolBox (University of Freiburg) for plasmids and/or strains. This research was supported by the Canton of Fribourg and the Swiss National Science Foundation (J.D. and C.D.V.).

## AUTHOR CONTRIBUTIONS

Conceptualization, R.H. and C.D.V.; Methodology, R.H., M.-P.P.-G., Z.H., M.J., G.M.G.O., A.S., J.D., and C.D.V.; Investigation, R.H., M.-P.P.-G., Z.H., M.J., G.M.G.O., and A.S.; Writing – Original Draft, C.D.V.; Writing – Review & Editing, R.H., M.-P.P.-G., J.D., and C.D.V.; Funding Acquisition, Resources, & Supervision, J.D. and C.D.V.

## DECLARATION OF INTERESTS

The authors declare no competing interests.

Received: July 30, 2018

Revised: October 3, 2018

Accepted: October 25, 2018

Published: December 6, 2018

## REFERENCES

- Albert, V., and Hall, M.N. (2015). mTOR signaling in cellular and organismal energetics. *Curr. Opin. Cell Biol.* 33, 55–66.
- Babu, P., Deschenes, R.J., and Robinson, L.C. (2004). Akr1p-dependent palmitoylation of Yck2p yeast casein kinase 1 is necessary and sufficient for plasma membrane targeting. *J. Biol. Chem.* 279, 27138–27147.
- Betz, C., and Hall, M.N. (2013). Where is mTOR and what is it doing there? *J. Cell Biol.* 203, 563–574.
- Binda, M., Péli-Gulli, M.P., Bonfils, G., Panchaud, N., Urban, J., Sturgill, T.W., Loewith, R., and De Virgilio, C. (2009). The Vam6 GEF controls TORC1 by activating the EGO complex. *Mol. Cell* 35, 563–573.
- Boeckstaens, M., Llinares, E., Van Vooren, P., and Marini, A.M. (2014). The TORC1 effector kinase Npr1 fine tunes the inherent activity of the Mep2 ammonium transport protein. *Nat. Commun.* 5, 3101.
- Bonifacino, J.S., and Traub, L.M. (2003). Signals for sorting of transmembrane proteins to endosomes and lysosomes. *Annu. Rev. Biochem.* 72, 395–447.
- Bowers, K., and Stevens, T.H. (2005). Protein transport from the late Golgi to the vacuole in the yeast *Saccharomyces cerevisiae*. *Biochim. Biophys. Acta* 1744, 438–454.
- Burd, C.G., and Emr, S.D. (1998). Phosphatidylinositol(3)-phosphate signaling mediated by specific binding to RING FYVE domains. *Mol. Cell* 2, 157–162.
- Cingolani, P., Patel, V.M., Coon, M., Nguyen, T., Land, S.J., Ruden, D.M., and Lu, X. (2012a). Using *Drosophila melanogaster* as a model for genotoxic chemical mutational studies with a new program, SnpSift. *Front. Genet.* 3, 35.
- Cingolani, P., Platts, A., Wang, L., Coon, M., Nguyen, T., Wang, L., Land, S.J., Lu, X., and Ruden, D.M. (2012b). A program for annotating and predicting the effects of single nucleotide polymorphisms, SnpEff: SNPs in the genome of *Drosophila melanogaster* strain w1118; iso-2; iso-3. *Fly (Austin)* 6, 80–92.
- Cowles, C.R., Odorizzi, G., Payne, G.S., and Emr, S.D. (1997). The AP-3 adaptor complex is essential for cargo-selective transport to the yeast vacuole. *Cell* 91, 109–118.
- Cox, J., and Mann, M. (2008). MaxQuant enables high peptide identification rates, individualized p.p.b.-range mass accuracies and proteome-wide protein quantification. *Nat. Biotechnol.* 26, 1367–1372.
- Dauner, K., Eid, W., Raghupathy, R., Presley, J.F., and Zha, X. (2017). mTOR complex 1 activity is required to maintain the canonical endocytic recycling pathway against lysosomal delivery. *J. Biol. Chem.* 292, 5737–5747.
- Day, K.J., Casler, J.C., and Glick, B.S. (2018). Budding yeast has a minimal endomembrane system. *Dev. Cell* 44, 56–72.



- Demetriades, C., Doumpas, N., and Telemann, A.A. (2014). Regulation of TORC1 in response to amino acid starvation via lysosomal recruitment of TSC2. *Cell* 156, 786–799.
- Dobzinski, N., Chuartzman, S.G., Kama, R., Schuldiner, M., and Gerst, J.E. (2015). Starvation-dependent regulation of Golgi quality control links the TOR signaling and vacuolar protein sorting pathways. *Cell Rep.* 12, 1876–1886.
- Dubouloz, F., Deloche, O., Wanke, V., Cameroni, E., and De Virgilio, C. (2005). The TOR and EGO protein complexes orchestrate microautophagy in yeast. *Mol. Cell* 19, 15–26.
- Eltschinger, S., and Loewith, R. (2016). TOR complexes and the maintenance of cellular homeostasis. *Trends Cell Biol.* 26, 148–159.
- Fan, S.J., Snell, C., Turley, H., Li, J.L., McCormick, R., Perera, S.M., Heublein, S., Kazi, S., Azad, A., Wilson, C., et al. (2016). PAT4 levels control amino-acid sensitivity of rapamycin-resistant mTORC1 from the Golgi and affect clinical outcome in colorectal cancer. *Oncogene* 35, 3004–3015.
- Forgac, M. (2007). Vacuolar ATPases: rotary proton pumps in physiology and pathophysiology. *Nat. Rev. Mol. Cell Biol.* 8, 917–929.
- Gao, M., and Kaiser, C.A. (2006). A conserved GTPase-containing complex is required for intracellular sorting of the general amino-acid permease in yeast. *Nat. Cell Biol.* 8, 657–667.
- Hayakawa, A., Hayes, S.J., Lawe, D.C., Sudharshan, E., Tuft, R., Fogarty, K., Lambright, D., and Corvera, S. (2004). Structural basis for endosomal targeting by FYVE domains. *J. Biol. Chem.* 279, 5958–5966.
- Henne, W.M., Buchkovich, N.J., and Emr, S.D. (2011). The ESCRT pathway. *Dev. Cell* 21, 77–91.
- Hinners, I., and Tooze, S.A. (2003). Changing directions: clathrin-mediated transport between the Golgi and endosomes. *J. Cell Sci.* 116, 763–771.
- Hurley, J.H., Im, Y.J., Lee, H.H., Ren, X., Wollert, T., and Yang, D. (2009). Piecing together the ESCRTs. *Biochem. Soc. Trans.* 37, 161–166.
- Jewell, J.L., and Guan, K.L. (2013). Nutrient signaling to mTOR and cell growth. *Trends Biochem. Sci.* 38, 233–242.
- Jin, N., Mao, K., Jin, Y., Tevzadze, G., Kauffman, E.J., Park, S., Bridges, D., Loewith, R., Saltiel, A.R., Klionsky, D.J., and Weisman, L.S. (2014). Roles for PI(3,5)P<sub>2</sub> in nutrient sensing through TORC1. *Mol. Biol. Cell* 25, 1171–1185.
- Jones, C.B., Ott, E.M., Keener, J.M., Curtiss, M., Sandrin, V., and Babst, M. (2012). Regulation of membrane protein degradation by starvation-response pathways. *Traffic* 13, 468–482.
- Joshi, N.A., and Fass, J.N. (2011). Sickle: a sliding-window, adaptive, quality-based trimming tool for FastQ file (Version 1.33). <https://github.com/najoshi/sickle>.
- Kamada, Y., Yoshino, K., Kondo, C., Kawamata, T., Oshiro, N., Yonezawa, K., and Ohsumi, Y. (2010). Tor directly controls the Atg1 kinase complex to regulate autophagy. *Mol. Cell Biol.* 30, 1049–1058.
- Kim, A., and Cunningham, K.W. (2015). A LAPF/phafin1-like protein regulates TORC1 and lysosomal membrane permeabilization in response to endoplasmic reticulum membrane stress. *Mol. Biol. Cell* 26, 4631–4645.
- Kim, E., Goraksha-Hicks, P., Li, L., Neufeld, T.P., and Guan, K.L. (2008). Regulation of TORC1 by Rag GTPases in nutrient response. *Nat. Cell Biol.* 10, 935–945.
- Kira, S., Tabata, K., Shirahama-Noda, K., Nozoe, A., Yoshimori, T., and Noda, T. (2014). Reciprocal conversion of Gtr1 and Gtr2 nucleotide-binding states by Npr2-Npr3 inactivates TORC1 and induces autophagy. *Autophagy* 10, 1565–1578.
- Kira, S., Kumano, Y., Ukai, H., Takeda, E., Matsuura, A., and Noda, T. (2016). Dynamic relocation of the TORC1-Gtr1/2-Ego1/2/3 complex is regulated by Gtr1 and Gtr2. *Mol. Biol. Cell* 27, 382–396.
- Klionsky, D.J., and Emr, S.D. (1989). Membrane protein sorting: biosynthesis, transport and processing of yeast vacuolar alkaline phosphatase. *EMBO J.* 8, 2241–2250.
- Kuhlee, A., Raunser, S., and Ungermann, C. (2015). Functional homologies in vesicle tethering. *FEBS Lett.* 589 (19 Pt A), 2487–2497.
- Li, H. (2011). A statistical framework for SNP calling, mutation discovery, association mapping and population genetical parameter estimation from sequencing data. *Bioinformatics* 27, 2987–2993.
- Li, H., and Durbin, R. (2010). Fast and accurate long-read alignment with Burrows-Wheeler transform. *Bioinformatics* 26, 589–595.
- Liu, Q., Xu, C., Kirubakaran, S., Zhang, X., Hur, W., Liu, Y., Kwiatkowski, N.P., Wang, J., Westover, K.D., Gao, P., et al. (2013). Characterization of Torin2, an ATP-competitive inhibitor of mTOR, ATM, and ATR. *Cancer Res.* 73, 2574–2586.
- MacGurn, J.A., Hsu, P.C., Smolka, M.B., and Emr, S.D. (2011). TORC1 regulates endocytosis via Npr1-mediated phosphoinhibition of a ubiquitin ligase adaptor. *Cell* 147, 1104–1117.
- Marat, A.L., and Haucke, V. (2016). Phosphatidylinositol 3-phosphates-at the interface between cell signalling and membrane traffic. *EMBO J.* 35, 561–579.
- Michel, A.H., Hatakeyama, R., Kimmig, P., Arter, M., Peter, M., Matos, J., De Virgilio, C., and Kornmann, B. (2017). Functional mapping of yeast genomes by saturated transposition. *eLife* 6, e23570.
- Morvan, J., Rinaldi, B., and Friant, S. (2012). Pkh1/2-dependent phosphorylation of Vps27 regulates ESCRT-I recruitment to endosomes. *Mol. Biol. Cell* 23, 4054–4064.
- Nadolski, M.J., and Linder, M.E. (2009). Molecular recognition of the palmitoylation substrate Vac8 by its palmitoyltransferase Pfa3. *J. Biol. Chem.* 284, 17720–17730.
- Oku, M., Maeda, Y., Kagohashi, Y., Kondo, T., Yamada, M., Fujimoto, T., and Sakai, Y. (2017). Evidence for ESCRT- and clathrin-dependent microautophagy. *J. Cell Biol.* 216, 3263–3274.
- Ong, S.E., Blagoev, B., Kratchmarova, I., Kristensen, D.B., Steen, H., Pandey, A., and Mann, M. (2002). Stable isotope labeling by amino acids in cell culture, SILAC, as a simple and accurate approach to expression proteomics. *Mol. Cell Proteomics* 1, 376–386.
- Pedruzzi, I., Dubouloz, F., Cameroni, E., Wanke, V., Roosen, J., Winderickx, J., and De Virgilio, C. (2003). TOR and PKA signaling pathways converge on the protein kinase Rim15 to control entry into G<sub>0</sub>. *Mol. Cell* 12, 1607–1613.
- Péli-Gulli, M.P., Sardou, A., Panchaud, N., Raucchi, S., and De Virgilio, C. (2015). Amino acids stimulate TORC1 through Lst4-Lst7, a GTPase-activating protein complex for the Rag family GTPase Gtr2. *Cell Rep.* 13, 1–7.
- Powis, K., and De Virgilio, C. (2016). Conserved regulators of Rag GTPases orchestrate amino acid-dependent TORC1 signaling. *Cell Discov.* 2, 15049.
- Powis, K., Zhang, T., Panchaud, N., Wang, R., De Virgilio, C., and Ding, J. (2015). Crystal structure of the Ego1-Ego2-Ego3 complex and its role in promoting Rag GTPase-dependent TORC1 signaling. *Cell Res.* 25, 1043–1059.
- Prouteau, M., Desfosses, A., Sieben, C., Bourgoin, C., Lydia Mozaffari, N., Demurtas, D., Mitra, A.K., Guichard, P., Manley, S., and Loewith, R. (2017). TORC1 organized in inhibited domains (TOROIDs) regulate TORC1 activity. *Nature* 550, 265–269.
- Puri, C., Vicinanza, M., Ashkenazi, A., Gratian, M.J., Zhang, Q., Bento, C.F., Renna, M., Menzies, F.M., and Rubinstein, D.C. (2018). The RAB11A-positive compartment is a primary platform for autophagosome assembly mediated by WIP1 recognition of PI3P-RAB11A. *Dev. Cell* 45, 114–131.
- Reinke, A., Chen, J.C., Aronova, S., and Powers, T. (2006). Caffeine targets TOR complex I and provides evidence for a regulatory link between the FRB and kinase domains of Tor1p. *J. Biol. Chem.* 281, 31616–31626.
- Sancak, Y., Peterson, T.R., Shaul, Y.D., Lindquist, R.A., Thoreen, C.C., Bar-Peled, L., and Sabatini, D.M. (2008). The Rag GTPases bind raptor and mediate amino acid signaling to mTORC1. *Science* 320, 1496–1501.
- Sancak, Y., Bar-Peled, L., Zoncu, R., Markhard, A.L., Nada, S., and Sabatini, D.M. (2010). Ragulator-Rag complex targets mTORC1 to the lysosomal surface and is necessary for its activation by amino acids. *Cell* 141, 290–303.
- Saxton, R.A., and Sabatini, D.M. (2017). mTOR signaling in growth, metabolism, and disease. *Cell* 168, 960–976.

- Sikorski, R.S., and Hieter, P. (1989). A system of shuttle vectors and yeast host strains designed for efficient manipulation of DNA in *Saccharomyces cerevisiae*. *Genetics* 122, 19–27.
- Sturgill, T.W., Cohen, A., Diefenbacher, M., Trautwein, M., Martin, D.E., and Hall, M.N. (2008). TOR1 and TOR2 have distinct locations in live cells. *Eukaryot. Cell* 7, 1819–1830.
- Suzuki, K., Kirisako, T., Kamada, Y., Mizushima, N., Noda, T., and Ohsumi, Y. (2001). The pre-autophagosomal structure organized by concerted functions of APG genes is essential for autophagosome formation. *EMBO J.* 20, 5971–5981.
- Suzuki, K., Akioka, M., Kondo-Kakuta, C., Yamamoto, H., and Ohsumi, Y. (2013). Fine mapping of autophagy-related proteins during autophagosome formation in *Saccharomyces cerevisiae*. *J. Cell Sci.* 126, 2534–2544.
- Takeda, E., Jin, N., Itakura, E., Kira, S., Kamada, Y., Weisman, L.S., Noda, T., and Matsuura, A. (2018). Vacuole-mediated selective regulation of TORC1-Sch9 signaling following oxidative stress. *Mol. Biol. Cell* 29, 510–522.
- Tanigawa, M., and Maeda, T. (2017). An *in vitro* TORC1 kinase assay that recapitulates the Gtr-independent glutamine-responsive TORC1 activation mechanism on yeast vacuoles. *Mol. Cell. Biol.* 37, e00075–17.
- Thoms, M., Mitterer, V., Kater, L., Falquet, L., Beckmann, R., Kressler, D., and Hurt, E. (2018). Suppressor mutations in Rpf2-Rrs1 or Rpl5 bypass the Cgr1 function for pre-ribosomal 5S RNP-rotation. *Nat. Commun.* 9, 4094.
- Ukai, H., Araki, Y., Kira, S., Oikawa, Y., May, A.I., and Noda, T. (2018). Gtr/Ego-independent TORC1 activation is achieved through a glutamine-sensitive interaction with Pib2 on the vacuolar membrane. *PLoS Genet.* 14, e1007334.
- Urban, J., Soulard, A., Huber, A., Lippman, S., Mukhopadhyay, D., Deloche, O., Wanke, V., Anrather, D., Ammerer, G., Riezman, H., et al. (2007). Sch9 is a major target of TORC1 in *Saccharomyces cerevisiae*. *Mol. Cell* 26, 663–674.
- Varlakhanova, N.V., Mihalevic, M.J., Bernstein, K.A., and Ford, M.G.J. (2017). Pib2 and the EGO complex are both required for activation of TORC1. *J. Cell Sci.* 130, 3878–3890.
- Wiśniewski, J.R., Zougman, A., Nagaraj, N., and Mann, M. (2009). Universal sample preparation method for proteome analysis. *Nat. Methods* 6, 359–362.
- Yamamoto, H., Fujioka, Y., Suzuki, S.W., Noshiro, D., Suzuki, H., Kondo-Kakuta, C., Kimura, Y., Hirano, H., Ando, T., Noda, N.N., and Ohsumi, Y. (2016). The intrinsically disordered protein Atg13 mediates supramolecular assembly of autophagy initiation complexes. *Dev. Cell* 38, 86–99.
- Yang, H., Jiang, X., Li, B., Yang, H.J., Miller, M., Yang, A., Dhar, A., and Pavletich, N.P. (2017). Mechanisms of mTORC1 activation by RHEB and inhibition by PRAS40. *Nature* 552, 368–373.
- Zarei, M., Sprenger, A., Rackiewicz, M., and Dengjel, J. (2016). Fast and easy phosphopeptide fractionation by combinatorial ERLIC-SCX solid-phase extraction for in-depth phosphoproteome analysis. *Nat. Protoc.* 11, 37–45.
- Zhu, L., Jorgensen, J.R., Li, M., Chuang, Y.S., and Emr, S.D. (2017). ESCRTs function directly on the lysosome membrane to downregulate ubiquitinated lysosomal membrane proteins. *eLife* 6, e26403.
- Zoncu, R., Bar-Peled, L., Efeyan, A., Wang, S., Sancak, Y., and Sabatini, D.M. (2011). mTORC1 senses lysosomal amino acids through an inside-out mechanism that requires the vacuolar H<sup>+</sup>-ATPase. *Science* 334, 678–683.

## STAR★METHODS

### KEY RESOURCES TABLE

REAGENT or RESOURCE	SOURCE	IDENTIFIER
<b>Antibodies</b>		
Rabbit anti-Sch9-pThr <sup>737</sup> (1:10'000)	De Virgilio lab	N/A
Goat anti-Sch9 (1:1'000)	De Virgilio lab	N/A
Mouse anti-GFP (1:1'000)	Roche	118144600001; RRID: AB_390913
Rabbit anti-Vps27 (1:1'000)	De Virgilio lab	N/A
Rabbit anti-Adh1 (1:200'000)	Calbiochem	126745
Goat anti-rabbit IgG-HRP conjugate (1:3'000)	BIO-RAD	170-6515; RRID: AB_11125142
Goat anti-mouse IgG-HRP conjugate (1:3'000)	BIO-RAD	170-6516; RRID: AB_11125547
Rabbit anti-goat IgG-HRP conjugate (1:5'000)	Abcam	ab6741; RRID: AB_955424
<b>Bacterial and Virus Strains</b>		
<i>E. coli</i> Rosetta (DE3)	Novagen	70954
<i>E. coli</i> DH5 $\alpha$	CGSC	12384
<b>Chemicals, Peptides, and Recombinant Proteins</b>		
$\gamma$ -[ <sup>18</sup> O <sub>4</sub> ]-ATP	Cambridge Isotope Laboratories	OLM-7858-20
$\gamma$ -[ <sup>32</sup> P]-ATP	Hartmann	SCP301
10 kD MW cutoff filter	PALL	OD010C34
30 kD MW cutoff filter	PALL	OD030C34
Arg10	Cambridge Isotope Laboratories	CNLM-539-H
Arg6	Cambridge Isotope Laboratories	CLM-2265-H
C8 disc	3M Empore	14-386
Cycloheximide	Applchem	10020730
FM4-64	Invitrogen	T3166
GFP-Trap_MA	Chromotek	gtma-400
IgG coupled to Dynabeads (M-270 Epoxy)	Thermo Fisher	14304
Lys4	Cambridge Isotope Laboratories	DLM-2640
Lys8	Cambridge Isotope Laboratories	CNLM-291-H
Ni-NTA beads	QIAGEN	30210
Pefabloc	Sigma-Aldrich	76307
Phos-tag	Wako	AAL-107
PhosSTOP	Roche	04-906-837-001
Rapamycin	LC Laboratories	R-5000
Roche Protease Inhibitor Cocktail	Roche	11-697-498-001
TFA	Sigma-Aldrich	302031-100ML
Titanium dioxide	GL Sciences	5020-75010
Torin2	Sigma-Aldrich	SML1224
Trypsin	Promega	V5113
Wortmannin	LC Laboratories	W-2990
Yeast nitrogen base	CONDA	1553.00

(Continued on next page)

**Continued**

REAGENT or RESOURCE	SOURCE	IDENTIFIER
Critical Commercial Assays		
Radiance Plus Sensitive ECL	Azure Biosystems	AC2103
ECL Western Blotting Detection	GE Healthcare	RPN2106
Deposited Data		
Original Data	Mendeley Data	<a href="http://dx.doi.org/10.17632/m9s42s94fc.1">http://dx.doi.org/10.17632/m9s42s94fc.1</a>
Experimental Models: Organisms/Strains		
YL516 (Figures 3A–3F, 4A, 4D, 4G, 5E, 6E, S2B–S2D, and S2F)	Binda et al., 2009	[BY4741/2] MATa; <i>his3Δ1</i> , <i>leu2Δ0</i> , <i>ura3Δ0</i>
RKH329 (Figures 1A and 2A)	This study	[YL516] <i>EGO1-GFP::HIS3</i>
RKH352 (Figure 1A)	This study	[RKH329] <i>apl5Δ::KanMX</i>
RKH346 (Figure 1A)	This study	[RKH329] <i>apl6Δ::KanMX</i>
RKH348 (Figure 1A)	This study	[RKH329] <i>vps41Δ::KanMX</i>
RKH338 (Figure 1A)	This study	[RKH329] <i>vam6Δ::KanMX</i>
RKH94 (Figures 1B, 2B, 2E, and 6B)	This study	[YL516] <i>GFP-GTR1</i>
RKH356 (Figure 1B)	This study	[RKH94] <i>apl5Δ::KanMX</i>
RKH330 (Figure 1B)	This study	[RKH94] <i>apl6Δ::KanMX</i>
RKH332 (Figure 1B)	This study	[RKH94] <i>vps41Δ::KanMX</i>
RKH334 (Figure 1B)	This study	[RKH94] <i>vam6Δ::KanMX</i>
SKY222 (Figures 1C, 2C, and 2F)	Kira et al., 2014	[BY4741] MATa; <i>his3Δ1</i> , <i>leu2Δ0</i> , <i>ura3Δ0</i> , <i>met15Δ0</i> , <i>LEU2::GFP-TOR1</i>
RKH358 (Figure 1C)	This study	[SKY222] <i>apl5Δ::KanMX</i>
RKH319 (Figure 1C)	This study	[SKY222] <i>apl6Δ::KanMX</i>
RKH324 (Figure 1C)	This study	[SKY222] <i>vps41Δ::KanMX</i>
RKH336 (Figure 1C)	This study	[SKY222] <i>vam6Δ::KanMX</i>
RKH388 (Figure 1D)	This study	[RKH329] <i>apl5Δ::KanMX pep12Δ::hphNT1</i>
RKH85 (Figures 1E and 3E)	This study	N/A[YL516] <i>ego1Δ::KanMX</i>
RKH353 (Figure 2A)	This study	[RKH329] <i>apl2Δ::KanMX</i>
RKH344 (Figure 2A)	This study	[RKH329] <i>apl4Δ::KanMX</i>
RKH364 (Figure 2A)	This study	[RKH329] <i>gga1Δ::KanMX gga2Δ::hphNT1</i>
RKH357 (Figure 2B)	This study	[RKH94] <i>apl2Δ::KanMX</i>
RKH340 (Figure 2B)	This study	[RKH94] <i>apl4Δ::KanMX</i>
RKH366 (Figure 2B)	This study	[RKH94] <i>gga1Δ::KanMX gga2Δ::hphNT1</i>
RKH372 (Figure 2C)	This study	[SKY222] <i>apl2Δ::KanMX</i>
RKH342 (Figure 2C)	This study	[SKY222] <i>apl4Δ::KanMX</i>
RKH368 (Figure 2C)	This study	[SKY222] <i>gga1Δ::KanMX gga2Δ::hphNT1</i>
YJU537 (Figure 2D)	Binda et al., 2009	[YL516] <i>EGO1-GFP::KanMX</i>
RKH390 (Figure 2G)	This study	[RKH329] <i>VPS27-mCherry::natMX4</i>
RKH104 (Figure 2H)	This study	[RKH94] <i>VPS27-mCherry::natMX4</i>
RKH309 (Figures 2I and S2E)	This study	[SKY222] <i>VPS27-mCherry::natMX4</i>
RKH375 (Figure 2J)	This study	[RKH329] <i>PIB2<sup>200</sup>-yEmRFP</i>
RKH383 (Figure 2K)	This study	[RKH94] <i>PIB2<sup>200</sup>-yEmRFP</i>
RKH362 (Figure 2L)	This study	[YL516] <i>LEU2::GFP-TOR1</i> , <i>PIB2<sup>200</sup>-yEmRFP</i>
MB32 (Figure 3D)	Binda et al., 2009	[YL516] <i>gtr1Δ::KanMX</i>
RKH106 (Figures 3D and S2B–S2D)	Michel et al., 2017	[YL516] <i>pib2Δ::KanMX</i>
MJA597-3C (Figures 4A and 4B)	This study	[YL516] <i>vph1Δ::KanMX</i>
MJA590-1B (Figures 4A and 4B)	This study	[YL516] <i>stv1Δ::hphNT1</i>
MJA589-1A (Figures 4A and 4B)	This study	[YL515] <i>vph1Δ::KanMX</i> , <i>stv1Δ::hphNT1</i>
MP52-2A (Figures 4C, 4D, 5E, and 6E)	Binda et al., 2009	[YL516] <i>tor1<sup>D330</sup>-3GFP</i>

(Continued on next page)



**Continued**

REAGENT or RESOURCE	SOURCE	IDENTIFIER
MP1632 (Figures 3E, 4E, 4G, and 5D)	This study	[YL516] <i>tor1Δ::KanMX</i>
RKH395 (Figures 4D and 6A)	This study	[YL516] <i>LEU2::GFP-TOR1</i>
RKH399 (Figure 4F)	This study	[YL516] <i>tco89Δ::KanMX, LEU2::GFP-TOR1</i>
RKH311 (Figures 4G and 4H)	This study	[YL516] <i>tco89Δ::KanMX</i>
RL170-2C (Figure 5B)	R. Loewith	[TB50] <i>TCO89-TAP::TRP1, leu2-3, ura3-52, trp1, his3, rme1</i>
RKH119 (Figures 5C, 5F, 5H, and S5)	This study	[YL516] <i>vps27Δ::KanMX</i>
MP5425 (Figure 5H)	This study	[RKH119] <i>pep4Δ::hphNT1</i>
RKH397 (Figures 5G and 5H)	This study	[RKH119] <i>his3Δ1::pHluorin-VPS27::SpHIS5</i>
RKH422 (Figures 5G and 5H)	This study	[RKH119] <i>his3Δ1::pHluorin-VPS27<sup>S155D/S157D/T159D/S274D/S277D/S279D/S280D</sup>::SpHIS5</i>
MP5427 (Figure 5H)	This study	[RKH397] <i>pep4Δ::hphNT1</i>
RKH452 (Figures 6C and 6E)	This study	[YL516] <i>tor1Δ::hphNT1, ATG13-EGFP::KanMX</i>
RKH401 (Figure 6D)	This study	[YL516] <i>ATG13-EGFP::HIS3</i>
RKH416 (Figure 6D)	This study	[YL516] <i>tor1<sup>D330</sup>-3GFP ATG13-EGFP::HIS3</i>
YL515 (Figure S1B)	<a href="#">Binda et al., 2009</a>	[BY4741/2] <i>MATα; his3Δ1, leu2Δ0, ura3Δ0</i>
KT1960	<a href="#">Pedruzzi et al., 2003</a>	<i>MATα; ura3-52, leu2, his3, trp1</i>
KT1961	<a href="#">Pedruzzi et al., 2003</a>	<i>MATα; ura3-52, leu2, his3, trp1</i>
GMGO003 (Figure S1A)	This study	[KT1960] <i>gtr1Δ::natMX4, HIS3::mCherry-ALP</i>
GMGO004 (Figure S1A)	This study	[KT1961] <i>gtr1Δ::natMX4, HIS3::mCherry-ALP</i>
GMGO023 (Figure S1A)	This study	[GMGO004] <i>ego1<sup>N175fs</sup></i>
GMGO024 (Figure S1A)	This study	[GMGO004] <i>ego3<sup>A49P</sup></i>
GMGO025 (Figure S1A)	This study	[GMGO004] <i>gtr2<sup>E42*</sup></i>
GMGO026 (Figure S1A)	This study	[GMGO003] <i>gtr2<sup>E185*</sup></i>
GMGO027 (Figure S1A)	This study	[GMGO004] <i>gtr2<sup>283fs</sup></i>
GMGO029 (Figure S1A)	This study	[GMGO004] <i>TOR1<sup>A1928D</sup></i>
GMGO030 (Figure S1A)	This study	[GMGO004] <i>tco89<sup>Q140fs</sup></i>
GMGO031 (Figure S1A)	This study	[GMGO003] <i>vps4<sup>N465fs</sup></i>
GMGO032 (Figure S1A)	This study	[GMGO003] <i>apm3<sup>W31*</sup></i>
GMGO033 (Figure S1A)	This study	[GMGO003] <i>akr1<sup>W725*</sup></i>
MB36-4B (Figure S1A)	This study	[BY4741/2] <i>MATα; gtr1Δ::kanMX, his3, leu2, ura3</i>
YAS063 (Figure S1A)	This study	[MB36-4B] <i>vps33<sup>L18P</sup></i>
YAS064 (Figure S1A)	This study	[MB36-4B] <i>ego1<sup>R9*</sup></i>
YAS066 (Figure S1A)	This study	[MB36-4B] <i>vps11<sup>Q76*</sup></i>
YAS067 (Figure S1A)	This study	[MB36-4B] <i>vam6<sup>Q391*</sup></i>
YAS068 (Figure S1A)	This study	[MB36-4B] <i>apl6<sup>M613R</sup></i>
YAS069 (Figure S1A)	This study	[MB36-4B] <i>apl6<sup>M1V</sup></i>
YAS070 (Figure S1A)	This study	[MB36-4B] <i>gtr2<sup>C231W</sup></i>
MB27 (Figure S1B)	<a href="#">Binda et al., 2009</a>	[YL515] <i>gtr1Δ::HIS3</i>
NP51-3C (Figure S1B)	<a href="#">Powis et al., 2015</a>	[MB27] <i>ego2Δ::KanMX</i>
GMGO010 (Figure S1B)	This study	[MB27] <i>tor1Δ::KanMX</i>
GMGO011 (Figure S1B)	This study	[MB27] <i>akr1Δ::KanMX</i>
GMGO012 (Figure S1B)	This study	[MB27] <i>vps11Δ::KanMX</i>
GMGO013 (Figure S1B)	This study	[MB27] <i>vps16Δ::KanMX</i>
GMGO014 (Figure S1B)	This study	[MB27] <i>vps18Δ::KanMX</i>
GMGO015 (Figure S1B)	This study	[MB27] <i>vps33Δ::KanMX</i>
GMGO016 (Figure S1B)	This study	[MB27] <i>vps41Δ::KanMX</i>
GMGO017 (Figure S1B)	This study	[MB27] <i>apl5Δ::KanMX</i>

(Continued on next page)

**Continued**

REAGENT or RESOURCE	SOURCE	IDENTIFIER
GMGO018 (Figure S1B)	This study	[MB27] <i>apl6Δ::KanMX6</i>
GMGO019 (Figure S1B)	This study	[MB27] <i>apm3Δ::KanMX</i>
GMGO020 (Figure S1B)	This study	[MB27] <i>aps3Δ::KanMX</i>
MP02-1B (Figure S1B)	This study	[YL516] <i>gtr1Δ::KanMX, tco89Δ::HIS3</i>
MP06-8B (Figure S1B)	Binda et al., 2009	[YL515] <i>gtr1Δ::KanMX, gtr2Δ::KanMX</i>
MP11-4C (Figure S1B)	This study	[YL516] <i>gtr1Δ::KanMX, vam6Δ::KanMX</i>
MP261-1D (Figure S1B)	This study	[YL515] <i>gtr1Δ::HIS3, ego1Δ::HIS3</i>
MP263-24C (Figure S1B)	This study	[YL516] <i>gtr1Δ::HIS3, ego3Δ::KanMX</i>
RKH157 (Figure S2B)	This study	[YL516] <i>PIB2<sup>120</sup>-EGFP</i>
RKH158 (Figures S2B and S2D)	This study	[YL516] <i>PIB2<sup>200</sup>-EGFP</i>
RKH159 (Figure S2B)	This study	[YL516] <i>PIB2<sup>350</sup>-EGFP</i>
RKH160 (Figure S2B)	This study	[YL516] <i>PIB2<sup>426</sup>-EGFP</i>
RKH161 (Figure S2B)	This study	[YL516] <i>PIB2<sup>532</sup>-EGFP</i>
RKH162 (Figures S2B and S2D)	This study	[YL516] <i>PIB2<sup>610</sup>-EGFP</i>
RKH323 (Figure S2C)	This study	[YL516] <i>PIB2<sup>200</sup>-yEmRFP</i>
RKH453 (Figure S2E)	This study	[RKH309] <i>ego1Δ::KanMX</i>
RKH386 (Figure S2F)	This study	[YL516] <i>gga1Δ::KanMX gga2Δ::hphNT1</i>
RKH439 (Figure S4)	This study	[BY4741/2] MATa; <i>vps27Δ::KanMX, his3Δ1, leu2Δ0, ura3Δ0, lys2Δ, arg4Δ::URA3</i>
Recombinant DNA		
pRS413 (Figures 1B, 1C, 1E, 2B, 2C, 2H, 2I, 2K, 2L, 3B, 3C, 4B, 4C, 4E, 4H, 5C–5F, 5H, 6A–6C, 6E, S1A, S1B, S2D–S2F, and S5)	Sikorski and Hieter, 1989	CEN/ARS, <i>HIS3</i>
pRS415 (Figures 1A, 1B, 1D, 1E, 2A, 2B, 2D, 2E, 2G, 2H, 2J, 2K, 3B–3F, 4A–4D, 4F–4H, 5F–5H, 6B–6E, S2D, S2F, and S5)	Sikorski and Hieter, 1989	CEN/ARS, <i>LEU2</i>
pRS416 (Figures 1A, 1B, 1D, 2A, 2B, 2D, 2E, 2G, 2H, 2J, 2K, 3A, 3C, 4B, 4C, 4F, 4H, 5C–5E, 5G, 5H, 6C–6E, S1A, S1B, and S2D)	Sikorski and Hieter, 1989	CEN/ARS, <i>URA3</i>
p1379 (Figures 1C, 2C, 2F, 2I, 2L, and S2E)	This study	CEN/ARS, <i>URA3, MET15</i>
pSK384 (Figures 1E and 3E)	Kira et al., 2016	CEN/ARS, <i>URA3, EGO1-GFP</i>
p3452 (Figures 1E and 3E)	This study	CEN/ARS, <i>URA3, EGO1<sup>L19A/L20A</sup>-GFP</i>
p3445 (Figures 2D–2F)	This study	CEN/ARS, <i>HIS3, ADH1p-RFP-VPS21</i>
p3485 (Figures 3A, 4B, 4F, and 4H)	This study	CEN/ARS, <i>HIS3, VPS27-mCherry</i>
p3027 (Figures 3A, 4B, 4E, and 4H)	This study	2μ, <i>LEU2, VAC8p-EEA1(human)<sup>1257-1411</sup>-GFP-SCH9<sup>709-824</sup></i>
p2976 (Figures 3B–3F, 4A, 4B, 4D, 4E, 4G, and 4H)	This study	2μ, <i>URA3, PRC1p-SCH9<sup>709-824</sup>-GFP-PHO8<sup>1-63</sup></i>
p2981 (Figures 3C–3F, 4A, 4D, and 4G)	This study	2μ, <i>HIS3, VAC8p-EEA1(human)<sup>1257-1411</sup>-GFP-SCH9<sup>709-824</sup></i>
p3047 (Figure 3E)	This study	2μ, <i>LEU2, PRC1p-SCH9<sup>709-824</sup>-GFP-PHO8<sup>1-63</sup></i>
p3400 (Figures 4E, 5D, 6C, and 6E)	This study	CEN/ARS, <i>HIS3, VAC8p-EEA1(human)<sup>1257-1411</sup>-yEmRFP-TOR1<sup>11954V</sup></i>
p3580 (Figures 4E, 6C, and 6E)	This study	CEN/ARS, <i>HIS3, VAC8p-yEmRFP-TOR1<sup>11954V</sup></i>
p3453 (Figure 5B; Table S1)	This study	[pET-28b(+)] <i>His<sub>6</sub>-HSE1</i>
p3454 (Figure 5B; Table S1)	This study	[pET-15b] <i>His<sub>6</sub>-VPS27</i>
p3509 (Figure 5B)	This study	[pET-15b] <i>His<sub>6</sub>-VPS27<sup>S155A/S157A/T159A/S274A/S277A/S279A/S280A/S339A/S494A/S495A</sup></i>
p3505 (Figures 5C–5F, 5H, and S5)	This study	CEN/ARS, <i>LEU2, VPS27</i>

(Continued on next page)

**Continued**

REAGENT or RESOURCE	SOURCE	IDENTIFIER
p3562 (Figure 5C)	This study	CEN/ARS, <i>LEU2</i> , <i>VPS27</i> <sup>S155D/S157D/T159D/S274D/S277D/S279D/S280D/S339D/S494D/S495D</sup>
p3550 (Figure 5F)	This study	CEN/ARS, <i>LEU2</i> , <i>VPS27</i> <sup>S155D/S157D/T159D/S274D/S277D/S279D/S280D</sup>
pRS426-GFP-ALP (Figures 5F and S5)	Cowles et al., 1997	2 $\mu$ , <i>URA3</i> , <i>GFP-PHO8</i>
pRS316-ATG13- <i>mCherry</i> (Figures 6A, 6B, and 6E)	Yamamoto et al., 2016	CEN/ARS, <i>URA3</i> , <i>ATG13-mCherry</i>
p3257 (Figure S2F)	This study	CEN/ARS, <i>URA3</i> , <i>PIB2</i> <sup>200</sup> -EGFP
pMB1580 (Figures S1A and S1B)	Binda et al., 2009	CEN/ARS, <i>LEU2</i> , <i>GAL1p-GST-gtr1</i> <sup>S20L</sup>
YCplac33- <i>EGO1-GST</i> (Figure S1A)	Powis et al., 2015	CEN/ARS, <i>URA3</i> , <i>EGO1-GST</i>
pSIVu- <i>EGO3-GFP</i> (Figure S1A)	This study	Integrative, <i>URA3</i> , <i>EGO3-EGFP</i>
pRS416- <i>GTR2-V5-HIS<sub>6</sub></i> (Figure S1A)	This study	CEN/ARS, <i>URA3</i> , <i>GTR2-V5-HIS<sub>6</sub></i>
pRS316- <i>TOR1-HA</i> (Figure S1A)	This study	CEN/ARS, <i>URA3</i> , <i>TOR1-HA</i>
YCplac33- <i>TCO89</i> (Figure S1A)	This study	CEN/ARS, <i>URA3</i> , <i>TCO89</i>
YEplac195- <i>GAL1-VAM6</i> (Figure S1A)	This study	2 $\mu$ , <i>URA3</i> , <i>GAL1p-VAM6</i>
BG1805- <i>GAL1-VPS41-TAP</i> (Figure S1A)	Open Biosystems	2 $\mu$ , <i>URA3</i> , <i>GAL1p-VPS41-TAP</i>
BG1805- <i>GAL1-VPS33-TAP</i> (Figure S1A)	Open Biosystems	2 $\mu$ , <i>URA3</i> , <i>GAL1p-VPS33-TAP</i>
BG1805- <i>GAL1-VPS11-TAP</i> (Figure S1A)	Open Biosystems	2 $\mu$ , <i>URA3</i> , <i>GAL1p-VPS11-TAP</i>
BG1805- <i>GAL1-APL6-TAP</i> (Figure S1A)	Open Biosystems	2 $\mu$ , <i>URA3</i> , <i>GAL1p-APL6-TAP</i>
YEplac195- <i>GAL1-APM3</i> (Figure S1A)	This study	2 $\mu$ , <i>URA3</i> , <i>GAL1p-APM3</i>
BG1805- <i>GAL1-AKR1-TAP</i> (Figure S1A)	Open Biosystems	2 $\mu$ , <i>URA3</i> , <i>GAL1p-AKR1-TAP</i>
p3457 (Figure S4)	This study	CEN/ARS, <i>HIS3</i> , <i>pHluorin-VPS27</i>
p3521 (Figure S5)	This study	CEN/ARS, <i>LEU2</i> , <i>VPS27</i> <sup>S155D/S157D/T159D</sup>
p3520 (Figure S5)	This study	CEN/ARS, <i>LEU2</i> , <i>VPS27</i> <sup>S274D/S277D/S279D/S280D</sup>
p3515 (Figure S5)	This study	CEN/ARS, <i>LEU2</i> , <i>VPS27</i> <sup>S339D</sup>
p3539 (Figure S5)	This study	CEN/ARS, <i>LEU2</i> , <i>VPS27</i> <sup>S494D/S495D</sup>
Software and Algorithms		
ImageJ	NIH	<a href="https://imagej.nih.gov/ij/">https://imagej.nih.gov/ij/</a>
FastQC v0.11.2		<a href="https://www.bioinformatics.babraham.ac.uk/projects/fastqc/">https://www.bioinformatics.babraham.ac.uk/projects/fastqc/</a>
Sickle v1.29	Joshi and Fass, 2011	<a href="https://github.com/najoshi/sickle">https://github.com/najoshi/sickle</a>
bwa mem v0.7.10	Li and Durbin, 2010	<a href="http://bio-bwa.sourceforge.net">http://bio-bwa.sourceforge.net</a>
Samtools v1.2	Li, 2011	<a href="http://samtools.sourceforge.net">http://samtools.sourceforge.net</a>
Bcftools v1.2	Li, 2011	<a href="http://samtools.sourceforge.net">http://samtools.sourceforge.net</a>
Snpeff v4.3	Cingolani et al., 2012b	<a href="http://snpeff.sourceforge.net">http://snpeff.sourceforge.net</a>
Snpsift	Cingolani et al., 2012a	<a href="http://snpeff.sourceforge.net/SnpSift.html">http://snpeff.sourceforge.net/SnpSift.html</a>
Photoshop	Adobe	<a href="https://www.adobe.com">https://www.adobe.com</a>
MaxQuant	Cox and Mann, 2008	<a href="http://www.biochem.mpg.de/5111795/maxquant">http://www.biochem.mpg.de/5111795/maxquant</a>

**CONTACT FOR REAGENT AND RESOURCE SHARING**

Further information and requests for resources and reagents should be directed to and will be fulfilled by the Lead Contact, Claudio De Virgilio ([Claudio.DeVirgilio@unifr.ch](mailto:Claudio.DeVirgilio@unifr.ch))

**EXPERIMENTAL MODEL AND SUBJECT DETAILS**

*Saccharomyces cerevisiae* strains used in this study are listed in the [Key Resources Table](#). They were grown as described in Method Details below. Recombinant His<sub>6</sub>-Vps27, His<sub>6</sub>-Vps27<sup>10A</sup>, and His<sub>6</sub>-Hse1 proteins were expressed in *Escherichia coli* Rosetta (DE3) and cloning procedures were carried out in *E. coli* DH5 $\alpha$ .

## METHOD DETAILS

### Yeast Strains, Plasmids, and Growth Conditions

*Saccharomyces cerevisiae* strains and plasmids are listed in [Key Resources Table](#). Unless otherwise stated, yeast strains were grown to mid-log phase in synthetic dextrose medium (0.17% yeast nitrogen base, 0.5% ammonium sulfate, and 2% glucose). For TORC1 activation by glutamine addition, cells were initially grown in synthetic dextrose-proline medium (0.17% yeast nitrogen base, 0.05% proline, and 2% glucose). Alternatively, synthetic dextrose medium lacking ammonium sulfate (SD-N) was used to starve cells for nitrogen and then restimulate them with glutamine. In [Figures 4A](#) and [4B](#), synthetic dextrose medium and synthetic dextrose medium lacking ammonium sulfate were buffered to pH 6.0 with 100 mM MES to support the growth of V-ATPase mutants. In all the experiments, prototrophic yeast strains were cultured at 30°C.

### Whole Genome Sequencing

Identification of suppressor mutations by high-throughput sequencing was carried out as recently described ([Thoms et al., 2018](#)). From the annotated and cured Variant Call Format (VCF) file, a manual reviewing of the variants was performed by checking UniProtKB and *Saccharomyces* Genome Database (SGD) annotations to select the candidate variants. In particular protein-protein or genetic interactions reporting a link to known members of the TORC1 pathway were favored. The variant effects predicted to be HIGH or MODERATE by SnpEff were also favored. The candidate variants were then validated both by complementation ([Figure S1A](#)) and gene deletion ([Figure S1B](#)) analyses.

### Fluorescence Microscopy

Where indicated, the vacuoles were visualized with the FM4-64 dye in the following manner. Yeast cells in mid-log phase were stained with 30  $\mu$ M (final concentration) of FM4-64 for 15 min, washed, resuspended in the original medium without FM4-64, and cultured for 40 min to allow FM4-64 to reach the vacuolar membranes. Images of live fluorescent cells were captured with an inverted spinning disk confocal microscope (VisiScope CSU-W1, Puchheim, Germany) that was equipped with a scientific grade 4.2 sCMOS camera and a 100  $\times$  1.3 NA oil immersion Nikon CFI series objective (Egg, Switzerland), and processed using ImageJ software.

### Cell Lysate Preparation and Immunoblot Analyses

Cells in mid-log phase were treated with 6.7% w/v trichloroacetic acid (final concentration), pelleted, washed with 99% acetone, dissolved in urea buffer (50 mM Tris-HCl [pH 8.0], 5 mM EDTA, 6 M urea, 1% SDS, Pefabloc, and PhosSTOP [one tablet per 10 mL]), and disrupted with glass beads using a Precellys homogenizer. After being heated at 65°C for 10 min in Laemmli SDS sample buffer, samples were subjected to SDS-PAGE and immunoblotting experiments using the indicated antibodies.

### Phos-tag Gel Analysis of Vps27 Isoforms

Protein extracts were prepared by glass bead disruption of cells resuspended in modified urea buffer (50 mM Tris [pH 7.5], 6 M Urea, 1% SDS, 0.4 mM Pefabloc, and 50 mM NaF). Following heat denaturation in Laemmli sample buffer at 65°C for 10 min, samples were run on 6% polyacrylamide gels containing 50  $\mu$ M Phos-tag (Wako Chemicals) according to the manufacturer's instructions. After blotting on nitrocellulose membranes, Vps27 phospho-isoforms were probed with rabbit polyclonal anti-Vps27 antibodies.

### Purification of Recombinant Vps27-Hse1 Complexes

His<sub>6</sub>-Vps27 (or His<sub>6</sub>-Vps27<sup>10D</sup>) and His<sub>6</sub>-Hse1 were co-expressed in and co-purified from bacteria (Rosetta strain). Expression was induced by 0.5 mM IPTG overnight at 16°C. Cells were lysed by sonication in lysis buffer (50 mM NaH<sub>2</sub>PO<sub>4</sub>, 300 mM NaCl, and 10 mM imidazole [pH 8.0]) and clarified by centrifugation in the presence of 0.1% NP40. The proteins were purified by incubation with Ni-NTA beads for 1 hr at 4°C, washed with wash buffer (50 mM NaH<sub>2</sub>PO<sub>4</sub>, 300 mM NaCl, and 50 mM imidazole [pH 8.0]), and eluted with elution buffer (50 mM NaH<sub>2</sub>PO<sub>4</sub>, 300 mM NaCl, and 250 mM imidazole [pH 8.0]).

### TORC1 Purification

The yeast strain expressing Tco89-TAP was grown in YPD until it reached OD<sub>600</sub> of 3.0. The medium was refreshed 1 hr prior to harvesting the cells, and TORC1 activity was further boosted by the addition of 25  $\mu$ g mL<sup>-1</sup> cycloheximide for 10 min. Cells were collected by filtration, passed through a syringe, frozen in liquid nitrogen, and disrupted with the grinding machine (Mixer Mill MM 400, Retsch). The obtained powder was resuspended in lysis buffer (50 mM HEPES/NaOH [pH 7.5], 5 mM CHAPS, 400 mM NaCl, 1 mM EDTA, 0.5 mM DTT, Pefabloc, and Roche protease inhibitor cocktail) and clarified by centrifugation. TORC1 was purified by incubation with the IgG-coupled Dynabeads for 2 hr at 4°C, washed with the wash buffer (50 mM HEPES [pH 7.5], 5 mM CHAPS, 400 mM NaCl, and 0.5 mM DTT), and cleaved off from the beads by TEV protease.



### **In Vitro TORC1 Kinase Assays**

28 µg of purified TORC1 was incubated with 5 µg of Vps27-Hse1 complex in kinase buffer (500 mM HEPES [pH 7.5], 120 mM NaCl, 0.6 mM DTT, 4 mM MgCl<sub>2</sub>, PhosSTOP [one tablet per 10 mL]), and 6 µM ATP for 20 min at 30°C. For autoradiography analyses, 10 µCi of [ $\gamma$ -<sup>32</sup>P]-ATP was also added. The reaction was stopped by adding Laemmli SDS sample buffer and boiling for 5 min.

### **In Vivo TORC1 Kinase Assays**

*In vivo* TORC1 kinase activity was assayed as previously described (Péli-Gulli et al., 2015), using phosphospecific anti-Sch9-pThr<sup>737</sup> and anti-Sch9 antibodies (GenScript) to probe endogenous Sch9. ET and VT activities were assayed with ET/VT reporters using phosphospecific anti-Sch9-pThr<sup>737</sup> and anti-GFP antibodies.

### **Filter-Aided In Vitro Kinase Assay and Phosphopeptide Enrichment**

To obtain maximal TORC1 activity, 30 µg of purified TORC1 was incubated with 1 mM MnCl<sub>2</sub> for 30 min. As a negative control, purified TORC1 was inhibited with 33.5 ng wortmannin for 30 min. Purified His<sub>6</sub>-Vps27, His<sub>6</sub>-Hse1, and TORC1 were added onto a 10 kD MW-cutoff filter (PALL) and incubated at 30°C for 1 hr in kinase buffer containing 50 mM HEPES (pH 7.4), 150 mM NaCl, 0.625 mM DTT, PhosSTOP<sup>TM</sup> [one tablet per 10 mL], 6.25 mM MgCl<sub>2</sub>, and 1.8 mM  $\gamma$ -[<sup>18</sup>O<sub>4</sub>]-ATP (Cambridge Isotope Laboratory, Andover, MA). The assay was quenched with 8 M urea and 1 mM DTT. Protein digestion for MS analysis was performed overnight according to a Filter Aided Sample Preparation (FASP) protocol (Wiśniewski et al., 2009). On the second day, the filter was transferred to a new tube and peptides were eluted twice with 100 µL 50 mM ammonium bicarbonate. The eluate was acidified with TFA to a final concentration of 1% prior phosphopeptide enrichment. For both *in vitro* and *in vivo* experiments, phosphopeptides were collected by metal oxide affinity enrichment using titanium dioxide (GL Sciences Inc., Tokyo, Japan). TiO<sub>2</sub> beads were pretreated with 300 mg mL<sup>-1</sup> lactic acid in 80% acetonitrile with 1% TFA (Zarei et al., 2016). Samples were incubated with a 2 mg TiO<sub>2</sub> slurry at room temperature for 30 min. TiO<sub>2</sub> beads were spun down and transferred onto a 200 µL pipette tip, which was blocked by a C8 disc (3M Empore). The tips were sequentially washed with 10% acetonitrile in 1% TFA, 80% acetonitrile in 1% TFA, and LC-MS grade water. Phosphopeptides were eluted with 50 µL of 5% ammonia in 20% acetonitrile and 50 µL of 5% ammonia in 40% acetonitrile. The eluate was mixed with 20 µL of 10% formic acid. Ammonium format was removed by vacuum concentration. The dried samples were resuspended in 20 µL of 0.1% formic acid for LC-MS/MS analysis. The tip flow-through was stored at -80°C for non-phosphopeptide analysis.

### **Sample Preparation of In Vivo SILAC Experiments**

The yeast strain (*vps27Δ lys2Δ arg4Δ*) expressing pHluorin-Vps27 was grown in synthetic dextrose complete medium containing either noncharged or charged lysine and arginine (Arg10, Arg6, Lys8, or Lys4 [Cambridge Isotope Laboratories]) and treated or not with 25 µg mL<sup>-1</sup> cycloheximide for 30 min. Dried TCA-treated cell pellets (50 mg) of each labeling were mixed. Cells were broken by glass beads in RIPA buffer containing 50 mM Tris-HCl (pH 7.5), 150 mM NaCl, 1 mM EDTA, 0.1% SDS, 0.1% sodium deoxycholate, and 1% NP-40. Debris were pelleted and the supernatant containing cellular proteins was collected as lysate. These steps were repeated 5 times to extract proteins. The lysate was incubated with 100 µL GFP-trap coupled to magnetic agarose beads (ChromoTek, Planegg-Martinsried, Germany) at 4°C overnight. To remove unspecific binding, beads were washed 3 times with modified RIPA buffer containing 1 mM EDTA, 0.1% sodium deoxycholate, 150 mM NaCl, 1% NP-40, and 50 mM Tris-HCl (pH 7.5). Beads were added onto the 30 kD MW-cutoff filter (PALL) and the buffer was exchanged to 50 mM ammonium bicarbonate (pH 8.0). Proteins were reduced with 1 mM DTT and alkylated with 5.5 mM iodoacetamide. Digestion was directly performed on beads with 20 µg trypsin (Promega, Dübendorf, Switzerland) overnight at 37°C. On the second day, the filter was transferred to a new tube and peptides were eluted twice with 100 µL 50 mM ammonium bicarbonate. The eluate was acidified with TFA to a final concentration of 1% prior phosphopeptide enrichment (see above).

### **Mass Spectrometry Analyses**

LC-MS/MS measurements were performed on a QExactive Plus and HF-X mass spectrometer coupled to an EasyLC 1000 and EasyLC 1200 nanoflow-HPLC, respectively. Peptides were separated on a fused silica HPLC-column tip (I.D. 75 µm, New Objective, self-packed with ReproSil-Pur 120 C18-AQ, 1.9 µm [Dr. Maisch, Ammerbuch, Germany] to a length of 20 cm) using a gradient of A (0.1% formic acid in water) and B (0.1% formic acid in 80% acetonitrile in water): loading of sample with 0% B with a flow rate of 600 nL min<sup>-1</sup>; separation ramp from 5%–30% B within 85 min with a flow rate of 250 nL min<sup>-1</sup>. NanoESI spray voltage was set to 2.3 kV and ion-transfer tube temperature to 250°C; no sheath and auxiliary gas was used. Mass spectrometers were operated in the data-dependent mode; after each MS scan (mass range  $m/z$  = 370 – 1750; resolution: 70'000 for QE Plus and 120'000 for HF-X) a maximum of ten, or twelve MS/MS scans were performed using a normalized collision energy of 25%, a target value of 1'000 (QE Plus)/5'000 (HF-X) and a resolution of 17'500 for QE Plus and 30'000 for HF-X. The MS raw files were analyzed using MaxQuant Software version 1.4.1.2 (Cox and Mann, 2008) for peak detection, quantification, and peptide identification using a full-length *S. cerevisiae* database (March, 2016) and common contaminants such as keratins and enzymes used for in-gel digestion as reference. Carbamidomethylcysteine was set as fixed modification and protein amino-terminal acetylation, serine-, threonine- and tyrosine-phosphorylation, and oxidation of methionine were set as variable modifications. The MS/MS tolerance was set to 20 ppm and three missed cleavages were allowed using trypsin/P as enzyme specificity. Peptide, site, and protein FDR based on a

forward-reverse database were set to 0.01, minimum peptide length was set to 7, and minimum number of peptides for identification of proteins was set to one, which must be unique. The “match-between-run” option was used with a time window of 1 min.

#### **QUANTIFICATION AND STATISTICAL ANALYSIS**

Statistical parameters are reported in the Figures and Figure Legends.

#### **DATA AND SOFTWARE AVAILABILITY**

Source data for gel images and graphs can be found in Mendeley Data: <http://dx.doi.org/10.17632/m9s42s94fc.1>.